Interception of two spheres with slip surfaces in linear Stokes flow

H. LUO[1] AND C. POZRIKIDIS[2]

[1]Department of Mechanical Engineering, George Washington University,
Suite T739, 801 22nd St. NW, Washington, DC 20052, USA

[2]Department of Mechanical and Aerospace Engineering, University of California, San Diego,
La Jolla, CA 92093-0411, USA

The interception of two spherical particles with arbitrary size in an infinite linear ambient Stokes flow is considered. The particle surfaces allow for slip according to the Navier–Maxwell–Basset law relating the shear stress to the tangential velocity. At any instant, the flow is computed in a frame of reference with origin at the centre of one particle using a cylindrical polar coordinate system whose axis of revolution passes through the centre of the second particle. Taking advantage of the axial symmetry of the boundaries of the flow in the particle coordinates, the problem is formulated as a system of integral equations for the zeroth, first, and second Fourier coefficients of the boundary traction with respect to the meridional angle. The force and torque exerted on each particle are determined by the zeroth and first Fourier coefficients, while the stresslet is determined by the zeroth, first, and second Fourier coefficients. The derived integral equations are solved with high accuracy using a boundary element method featuring adaptive element distribution and automatic time step adjustment according to the inter-particle gap. The results strongly suggest the existence of a critical value for the slip coefficient below which the surfaces of two particle collide after a finite interception time. The critical value depends on the relative initial particle positions. The particle stress tensor and coefficients of the linear and quadratic terms in the expansion of the effective viscosity of a dilute suspension in terms of the concentration in simple shear flow are discussed and evaluated. Surface slip significantly reduces the values of both coefficients and the longitudinal particle self-diffusivity.

1. Introduction

The interception of two spherical particles in a viscous flow has been discussed extensively in the literature as a prototype of particle interaction in a non-dilute and non-concentrated suspension. One objective has been to describe particle trajectories with reference to collision efficiency and permanent doublet formation. Accurate expressions describing these trajectories have been derived for a broad range of conditions, from remote to nearly touching interceptions, as reviewed by Jones & Schmitz (1988), Cichocki, Felderhof & Schmitz (1988), and Kim & Karrila (1991). Other theoretical studies have sought to estimate the particle shear and self-diffusivity and assess the effect of particle interaction on the rheological properties of a dilute suspension to second-order with respect to the particle volume fraction (Batchelor & Green 1972*a*, *b*). The results have shown that, both at first and second order, a suspension of spherical particles behaves like a Newtonian fluid with an increased effective viscosity.

In simple shear flow, two particles may approach from infinity, intercept, and resume their initial paths with some positive or negative delay. Particle doublets separated by a small distance may permanently engage in a periodic motion described by a closed orbit. Our inability to assess the percentage of particles exhibiting the second type of motion in the absence of Brownian fluctuations and surface roughness has frustrated the computation of the effective rheological properties at second order with respect to the particle volume fraction (Batchelor & Green 1972b). Surface roughness allows for soft collisions that modify the closed orbits, but the effect is not sufficiently strong to remove the indeterminacy of the particle pair distribution. Only when all particle pairs lie in a plane that is normal to the vorticity of the shear flow the problem becomes well-posed. Wilson & Davis (2000, 2002) considered situations where particles initially residing on closed orbits are moved onto open trajectories by roughness-mediated contact. Because of this exclusion, closed orbits do not arise at steady state and can be neglected in the study of the effective rheological properties. Such difficulties are not encountered in the case of particles convected in two-dimensional or axisymmetric purely elongational flow where closed orbits do not arise.

When the particle size is comparable to the mean free path of an ambient gas, the discrete nature of the fluid causes an apparent slip velocity over the particle surface. A liquid may also slide over a surface when the shear stress is high enough to overcome the fluid–solid molecular attraction forces, as it does near a three-phase contact line in relative motion with respect to the substrate. Slip velocity has been reported in the flow of liquids over hydrophobic and possibly more general surfaces, although the laboratory evidence is not conclusive (e.g. Vinogradova 1999). On the other hand, macromolecular solutions and melts are known to exhibit intermittent slip that is responsible for flow instability (Black & Graham 2001). In various physical systems, the slip length may vary from nanometres to micrometres. In engineering applications, slip occurs over the boundaries of porous materials (e.g. Beavers & Joseph 1967).

The slip boundary condition was first proposed by Navier (1823) and further discussed by Maxwell (1879) in the context of gas flow (e.g. Schaaf & Chambre 1961; Cercignani 2000). Basset (1888) derived an analytical solution for the flow due to a solid sphere translating in infinite fluid at low Reynolds numbers, and generalized the Stokes law for the drag force. Hocking (1973) considered the motion of a sphere toward a plane wall or another sphere and showed that, when slip is allowed on both surfaces, the resistive force becomes only logarithmically dependent on the gap, and contact is achieved at a finite time. In related studies, Felderhof (1976a, b), Schmitz & Felderhof (1978), and Felderhof & Jones (1986) used analytical techniques to study arbitrary Stokes flow past a slippery sphere. Schmitz & Felderhof (1982a, b, c) considered the grand resistance and mobility matrices for one or two porous spherical particles with arbitrary permeability.

Luo & Pozrikidis (2007) recently considered the motion of a single spherical particle in infinite unbounded linear flow and in semi-infinite simple shear flow bounded by a plane wall. In the case of infinite flow, they derived an exact solution using the singularity representation, and produced analytical expressions for the force, torque, and stresslet in terms of the slip coefficient. These results generalize the Stokes–Basset law for the force and the Einstein coefficient for the stresslet. The slip velocity was shown to reduce the drag force, torque, and the effective viscosity of a dilute suspension.

In this paper, we consider the interception of two spherical particles in an effectively infinite linear flow and propose a computational framework for computing the resistance coefficients and the translational and angular velocities of freely suspended

particles. The key idea is to take advantage of the axial symmetry of the boundaries of the flow with respect to the axis that passes through the particle centres at any instant, and thereby formulate the problem as a system of integral equations for the zeroth, first, and second Fourier coefficients of the boundary traction with respect to the meridional angle. For particles immersed in a linear flow, the force and torque exerted on each particle are determined by the zeroth and first Fourier coefficients, while the stresslet is determined by the zeroth, first, and second Fourier coefficients. The integral equations are solved with high accuracy using a boundary element method featuring an adaptive element distribution and adaptive time-stepping according to the inter-particle gap.

The problem is formulated in §2, the boundary integral formulation is discussed in §3, the integral equations for the Fourier coefficients are derived in §4, and the computation of the stresslet in terms of the Fourier coefficients is discussed in §5. In §6, numerical results are presented for particles intercepting in simple shear flow, and the effect of the particle slip on the effective viscosity of a dilute suspension and the longitudinal self-diffusivity are evaluated. The main contributions, conclusions, and prospects for further work are summarized in §7.

2. Problem statement and mathematical formulation

We consider viscous flow past two suspended spherical particles in an effectively infinite domain. Far from the particles, the velocity obtains the linear form

$$U^\infty(X) = L^T \cdot X, \tag{2.1}$$

where L is the velocity gradient tensor, the superscript T denotes the matrix transpose, and $X = (X, Y, Z)$ is the position in laboratory-fixed coordinates. The radius of the first particle is a, and the radius of the second particle is δa, where δ is the radii ratio. Without loss of generality, we assume $\delta \leqslant 1$. The presence or motion of the particles generates a disturbance flow, denoted by the superscript D, that may be added to the incident linear flow to yield the total flow with velocity $U = U^\infty + U^D$.

The no-penetration and slip boundary conditions are assumed over the particle surfaces, requiring

$$U = V^{(i)} + \Omega^{(i)} \times (X - X_c^{(i)}) + U^S, \tag{2.2}$$

where $V^{(i)}$ is the velocity of translation of the ith particle centre, $X_c^{(i)}$, and $\Omega^{(i)}$ is the angular velocity of rotation about $X_c^{(i)}$, for $i = 1, 2$. The slip velocity is given by the Navier–Maxwell–Basset relation,

$$U^S = \frac{L}{\mu \beta} N \times F \times N = \frac{\lambda}{\mu} N \times F \times N, \tag{2.3}$$

where μ is the fluid viscosity, $F \equiv \Sigma \cdot N$ is the traction, Σ is the stress tensor, N is the unit normal vector pointing into the fluid, L is a chosen length scale, and β is the dimensionless Basset (1888) slip coefficient ranging from zero corresponding to vanishing shear stress and perfect slip, to infinity corresponding to no slip; $\lambda = L/\beta$ is the particle surface slip length.

In the case of a rarified gas, the slip coefficient, β, and slip length, λ, can be rigorously related to the mean free path, λ_f, by the Maxwell relation $\lambda_f/\lambda = \beta Kn = \sigma/(2 - \sigma)$, where $Kn \equiv \lambda_f/L$ is the Knudsen number, and σ is tangential momentum accommodation coefficient (TMAC) expressing the fraction of molecules that undergo diffusive instead of specular reflection (e.g. Schaaf & Chambre 1961; Cercignani 2000).

The limit $\sigma = 1$ yields the no-slip boundary condition, $\beta \to \infty$, whereas the limit $\sigma = 0$ yields the perfect-slip boundary condition, $\beta \to 0$.

2.1. *Particle doublet coordinates*

To standardize the problem, we introduce a new coordinate system, (x, y, z), with origin at the centre of the first sphere, $X_c^{(1)}$. The x axis passes through the centres of the two particles, and the y and z axes point in two orthogonal but otherwise unspecified directions. Thus, the definition of the particle coordinate system affords one degree of freedom. The position vector and velocity transform according to the equations

$$X = X_c^{(1)} + A \cdot x, \qquad u = A^T \cdot U, \tag{2.4}$$

where A is an orthogonal transformation matrix whose columns host the direction cosines of the unit vectors along the x, y, and z axes,

$$A = \begin{bmatrix} (e_x)_X & (e_y)_X & (e_z)_X \\ (e_x)_Y & (e_y)_Y & (e_z)_Y \\ (e_x)_Z & (e_y)_Z & (e_z)_Z \end{bmatrix} \equiv \begin{bmatrix} A_{Xx} & A_{Xy} & A_{Xz} \\ A_{Yx} & A_{Yy} & A_{Yz} \\ A_{Zx} & A_{Zy} & A_{Zz} \end{bmatrix}, \tag{2.5}$$

where

$$e_x = \frac{X_c^{(2)} - X_c^{(1)}}{\left| X_c^{(2)} - X_c^{(1)} \right|}, \tag{2.6}$$

and $e_i \cdot e_j = \delta_{ij}$. Applying the velocity transformation rules for the incident linear flow, we find

$$u^\infty(x) = A^T \cdot L^T \cdot X = A^T \cdot L^T \cdot \left(X_c^{(1)} + A \cdot x \right) \tag{2.7}$$

or

$$u^\infty(x) = v^\infty + M^T \cdot x, \tag{2.8}$$

where

$$v^\infty = A^T \cdot L^T \cdot X_c^{(1)}, \qquad M = A^T \cdot L \cdot A. \tag{2.9}$$

The orthogonality of the matrix A ensures that the trace of M is zero.

2.2. *Simple shear flow*

In the particular case of simple shear flow along the Y axis with the velocity varying linearly in the X direction (figure 1), the velocity in the laboratory frame is given by

$$U_X^\infty = 0, \qquad U_Y^\infty = kX, \qquad U_Z^\infty = 0, \tag{2.10}$$

and the associated velocity gradient tensor is

$$L = k \begin{bmatrix} 0 & 1 & 0 \\ 0 & 0 & 0 \\ 0 & 0 & 0 \end{bmatrix}, \tag{2.11}$$

where k is the shear rate. Making substitutions, we find the velocity in the particle frame,

$$v_x^\infty = A_{Yx} X_c^{(1)}, \qquad v_y^\infty = A_{Yy} X_c^{(1)}, \qquad v_z^\infty = A_{Yz} X_c^{(1)}, \tag{2.12}$$
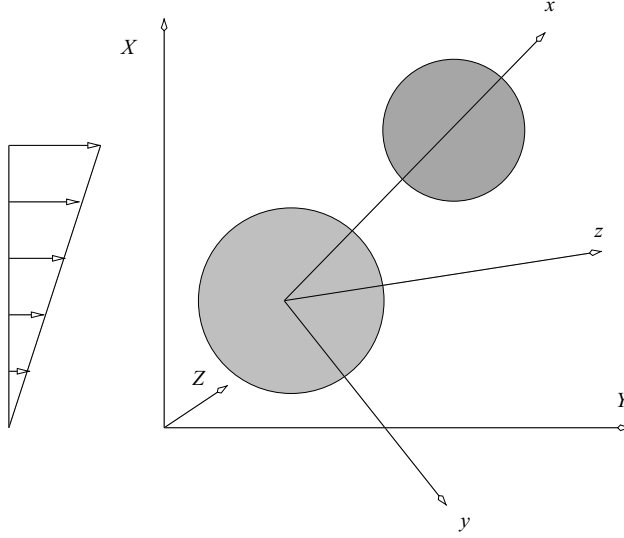
FIGURE 1. Two spherical particles with arbitrary radii intercepting in simple shear flow; (X, Y, Z) are the global coordinates and (x, y, z) are the particle doublet coordinates.

where

$$\boldsymbol{M}^T = k \begin{bmatrix} A_{Yx}A_{Xx} & A_{Yx}A_{Xy} & A_{Yx}A_{Xz} \\ A_{Yy}A_{Xx} & A_{Yy}A_{Xy} & A_{Yy}A_{Xz} \\ A_{Yz}A_{Xx} & A_{Yz}A_{Xy} & A_{Yz}A_{Xz} \end{bmatrix} = k\,\boldsymbol{r}_2 \otimes \boldsymbol{r}_1, \tag{2.13}$$

and $\boldsymbol{r}_1$, $\boldsymbol{r}_2$ are the first and second rows of $\boldsymbol{A}$.

When the axis connecting the particle centres is parallel to the XY plane, we set $A_{Zx}=0$ for the first unit vector, $A_{Xy}=-A_{Yx}$, $A_{Yy}=A_{Xx}$, $A_{Zy}=0$, for the second unit vector, and $A_{Xz}=0$, $A_{Yz}=0$, $A_{Zz}=1$, for the third unit vector, and find that the last row and column of $\boldsymbol{M}$ are zero, yielding

$$\boldsymbol{M}^T = k \begin{bmatrix} M_{11} & M_{12}-1 & 0 \\ M_{12} & -M_{11} & 0 \\ 0 & 0 & 0 \end{bmatrix}, \tag{2.14}$$

where $M_{11} = A_{Xx}A_{Yx}$, $M_{12} = A_{Xx}^2$. Thus,

$$\left. \begin{aligned} u_x^\infty &= v_x^\infty + kM_{11}x + k(M_{12}-1)y, \\ u_y^\infty &= v_y^\infty + kM_{12}x - kM_{11}y, \qquad u_z^\infty = 0. \end{aligned} \right\} \tag{2.15}$$

2.3. *Governing equations*

The Reynolds number written with respect to the particle size is assumed to be sufficiently small that the motion of the fluid is governed by the equations of Stokes flow,

$$-\nabla p + \mu \nabla^2 \boldsymbol{u} = \boldsymbol{0}, \qquad \nabla \cdot \boldsymbol{u} = 0, \tag{2.16}$$

where p is the pressure. The boundary conditions on the particle surfaces require

$$\boldsymbol{u} = \boldsymbol{u}^{RBM} + \boldsymbol{u}^S, \tag{2.17}$$

where

$$\boldsymbol{u}^{RBM} = \boldsymbol{v}^{(i)} + \boldsymbol{\omega}^{(i)} \times \left(\boldsymbol{x} - \boldsymbol{x}_c^{(i)}\right) \tag{2.18}$$

expresses rigid-body motion, $\boldsymbol{v}^{(i)}$ is the velocity of translation of the ith particle centre, $\boldsymbol{x}_c^{(i)}$, and $\boldsymbol{\omega}^{(i)}$ is the angular velocity of rotation about $\boldsymbol{x}_c^{(i)}$; by definition, $\boldsymbol{x}_c^{(1)} = \boldsymbol{0}$. The slip velocity is given by the Navier–Maxwell–Basset relation

$$\boldsymbol{u}^S = \frac{L}{\mu\beta}\boldsymbol{n} \times \boldsymbol{f} \times \boldsymbol{n} = \frac{\lambda}{\mu}\boldsymbol{n} \times \boldsymbol{f} \times \boldsymbol{n}, \tag{2.19}$$

where $\boldsymbol{f} \equiv \boldsymbol{\sigma} \cdot \boldsymbol{n}$ is the traction, $\boldsymbol{\sigma}$ is the stress tensor, and $\boldsymbol{n}$ is the unit normal vector pointing into the fluid.

The particle motion in the fixed frame is governed by the ordinary differential equations

$$\frac{\mathrm{d}\boldsymbol{X}_c^{(i)}}{\mathrm{d}t} = \boldsymbol{A} \cdot \boldsymbol{v}^{(i)}, \qquad \frac{\mathrm{d}\boldsymbol{D}^{(i)}}{\mathrm{d}t} = \left(\boldsymbol{A} \cdot \boldsymbol{\omega}^{(i)}\right) \times \boldsymbol{D}^{(i)}, \tag{2.20}$$

for $i = 1, 2$, where the particle director $\boldsymbol{D}^{(i)}$ is a material vector painted on each particle. Unless the rotation of a spherical particle is of interest, consideration of the second equation is not required.

3. Boundary integral formulation

The governing equations are solved in the particle doublet coordinates using the boundary integral formulation for Stokes flow. To begin, we decompose the flow in the particle frame into the undisturbed component denoted by the superscript ∞ and a disturbance component due to the particles denoted by the superscript D, and express the disturbance velocity at the point $\boldsymbol{x}_0$ that lies inside the fluid in terms of integrals over the particle surfaces, P,

$$\boldsymbol{u}^D(\boldsymbol{x}_0) = -\frac{1}{8\pi\mu}\mathscr{S}(\boldsymbol{x}_0, \boldsymbol{f}^D, P) + \frac{1}{8\pi}\mathscr{D}(\boldsymbol{x}_0, \boldsymbol{u}^D, P). \tag{3.1}$$

We have introduced the single- and double-layer potentials of Stokes flow defined over a generic surface, D,

$$\left.\begin{aligned}\mathscr{S}_j(\boldsymbol{x}_0, \boldsymbol{f}, D) &\equiv \iint_D f_i(\boldsymbol{x})G_{ij}(\boldsymbol{x}, \boldsymbol{x}_0)\,\mathrm{d}S(\boldsymbol{x}), \\ \mathscr{D}_j(\boldsymbol{x}_0, \boldsymbol{u}, D) &\equiv \iint_D u_i(\boldsymbol{x})T_{ijk}(\boldsymbol{x}, \boldsymbol{x}_0)n_k(\boldsymbol{x})\,\mathrm{d}S(\boldsymbol{x}),\end{aligned}\right\} \tag{3.2}$$

where

$$G_{ij}(\boldsymbol{x}, \boldsymbol{x}_0) = \frac{\delta_{ij}}{r} + \frac{\hat{x}_i\hat{x}_j}{r^3}, \qquad T_{ijk}(\boldsymbol{x}, \boldsymbol{x}_0) = -6\frac{\hat{x}_i\hat{x}_j\hat{x}_k}{r^5}, \tag{3.3}$$

are the free-space Green's function and associated stress tensors, $\hat{\boldsymbol{x}} = \boldsymbol{x} - \boldsymbol{x}_0$, $r = |\hat{\boldsymbol{x}}|$, and δ_{ij} is Kronecker's delta (e.g. Pozrikidis 1992). Next, we use the reciprocal theorem to write

$$-\frac{1}{8\pi\mu}\mathscr{S}(\boldsymbol{x}_0, \boldsymbol{f}^\infty, P) + \frac{1}{8\pi}\mathscr{D}(\boldsymbol{x}_0, \boldsymbol{u}^\infty, P) = 0, \tag{3.4}$$

and introduce the integral identity

$$\mathscr{D}(\boldsymbol{x}_0, \boldsymbol{u}^{RBM}, P) = 0. \tag{3.5}$$

Combining (3.1), (3.4) and (3.5), and enforcing the boundary conditions on the particles surfaces, we obtain

$$\boldsymbol{u}(\boldsymbol{x}_0) = \boldsymbol{u}^\infty(\boldsymbol{x}_0) - \frac{1}{8\pi\mu}\mathscr{S}(\boldsymbol{x}_0, \boldsymbol{f}, P) + \frac{1}{8\pi}\mathscr{D}(\boldsymbol{x}_0, \boldsymbol{u}^S, P). \qquad (3.6)$$

In the absence of slip velocity, the last term on the right-hand side does not appear.

To derive integral equations, we apply (3.6) at the surface of each particle and enforce the slip boundary condition to find

$$\mathscr{S}(\boldsymbol{x}_0, \boldsymbol{f}, P) - \mu\mathscr{D}^{PV}(\boldsymbol{x}_0, \boldsymbol{u}^S, P) = -8\pi\mu(\boldsymbol{u}^{RBM} - \boldsymbol{u}^\infty(\boldsymbol{x}_0)) - 4\pi\mu\boldsymbol{u}^S(\boldsymbol{x}_0), \qquad (3.7)$$

where PV denotes the principal-value integral. Complemented with (2.19), this equation provides us with a system of three scalar equations for the three components of the traction over the particle surfaces, also involving the particle translational and angular velocities.

3.1. *Fourier expansion*

A key observation is that the boundaries of the flow, but not the flow itself, are axially symmetric with respect to the x-axis. This geometrical property allows us to simplify the problem by expressing the cylindrical polar components of the left- and right-hand sides of (3.7), denoted as (x, σ, φ), in Fourier series with respect to the meridional angle, φ, where σ is the distance from the x axis, and φ is defined such that $y = \sigma\cos\varphi$ and $z = \sigma\sin\varphi$. We begin by writing

$$\begin{bmatrix} u_x^{RBM} \\ u_\sigma^{RBM} \\ u_\varphi^{RBM} \end{bmatrix} = \begin{bmatrix} v_x \\ 0 \\ \omega_x\sigma \end{bmatrix} + \begin{bmatrix} -\omega_z\sigma \\ v_y + \omega_z\tilde{x} \\ v_z - \omega_y\tilde{x} \end{bmatrix}\cos\varphi + \begin{bmatrix} \omega_y\sigma \\ v_z - \omega_y\tilde{x} \\ -(v_y + \omega_z\tilde{x}) \end{bmatrix}\sin\varphi, \qquad (3.8)$$

for the ith particle, where $\tilde{x} = x - x_c$, and

$$\begin{bmatrix} u_x^\infty \\ u_\sigma^\infty \\ u_\varphi^\infty \end{bmatrix} = \begin{bmatrix} v_x^\infty + M_{11}x \\ \frac{1}{2}(M_{22} + M_{33})\sigma \\ \frac{1}{2}(M_{23} - M_{32})\sigma \end{bmatrix} + \begin{bmatrix} M_{21}\sigma \\ v_y^\infty + M_{12}x \\ v_z^\infty + M_{13}x \end{bmatrix}\cos\varphi + \begin{bmatrix} M_{31}\sigma \\ v_z^\infty + M_{13}x \\ -v_y^\infty - M_{12}x \end{bmatrix}\sin\varphi$$

$$+ \frac{1}{2}\begin{bmatrix} 0 \\ (M_{22} - M_{33})\sigma \\ (M_{23} + M_{32})\sigma \end{bmatrix}\cos 2\varphi + \frac{1}{2}\begin{bmatrix} 0 \\ (M_{23} + M_{32})\sigma \\ (-M_{22} + M_{33})\sigma \end{bmatrix}\sin 2\varphi. \qquad (3.9)$$

Motivated by these forms, we express the cylindrical polar components of the velocity field in the truncated Fourier series

$$u_\alpha(x, \sigma, \varphi) = \mathscr{U}_{\alpha 0}(x, \sigma) + \sum_{m=1}^2 \left[\mathscr{U}_{\alpha m}^c(x, \sigma)\cos(m\varphi) + \mathscr{U}_{\alpha m}^s(x, \sigma)\sin(m\varphi)\right], \qquad (3.10)$$

where Greek indices take the values x, σ, φ, and $\mathscr{U}_{\alpha 0}$, $\mathscr{U}_{\alpha m}^c$ and $\mathscr{U}_{\alpha m}^s$ are Fourier coefficients. Similarly, we express the cylindrical polar components of the boundary traction in the truncated Fourier series

$$f_\alpha(x, \varphi) = \mathscr{F}_{\alpha 0}(x, \sigma) + \sum_{m=1}^2 \left[\mathscr{F}_{\alpha m}^c(x)\cos(m\varphi) + \mathscr{F}_{\alpha m}^s(x)\sin(m\varphi)\right], \qquad (3.11)$$

and $\mathscr{F}_{\alpha m}^c$, $\mathscr{F}_{\alpha m}^s$ are unknown cosine and sine Fourier coefficients. The Fourier expansion of the tangential component of the traction required for the evaluation of the

slip velocity is

$$(\boldsymbol{n} \times \boldsymbol{f} \times \boldsymbol{n})_\alpha = \mathscr{T}_{\alpha 0} + \sum_{m=1}^{2} \left[\mathscr{T}_{\alpha m}^c \cos(m\varphi) + \mathscr{T}_{\alpha m}^s \sin(m\varphi) \right], \qquad (3.12)$$

where

$$\mathscr{T}_{x0} = \frac{\sigma}{R^2}(\sigma \mathscr{F}_{x0} - \tilde{x}\mathscr{F}_{\sigma 0}), \quad \mathscr{T}_{\sigma 0} = -\frac{\tilde{x}}{R^2}(\sigma \mathscr{F}_{x0} - \tilde{x}\mathscr{F}_{\sigma 0}), \quad \mathscr{T}_{\varphi 0} = \mathscr{F}_{\varphi 0}, \qquad (3.13)$$

and

$$\left.\begin{aligned}
\mathscr{T}_{xm}^c &= \frac{\sigma}{R^2}\left(\sigma \mathscr{F}_{xm}^c - \tilde{x}\mathscr{F}_{\sigma m}^c\right), \quad \mathscr{T}_{\sigma m}^c = -\frac{\tilde{x}}{R^2}\left(\sigma \mathscr{F}_{xm}^c - \tilde{x}\mathscr{F}_{\sigma m}^c\right), \quad \mathscr{T}_{\varphi m}^c = \mathscr{F}_{\varphi m}^c, \\
\mathscr{T}_{xm}^s &= \frac{\sigma}{R^2}\left(\sigma \mathscr{F}_{xm}^s - \tilde{x}\mathscr{F}_{\sigma m}^s\right), \quad \mathscr{T}_{\sigma m}^s = -\frac{\tilde{x}}{R^2}\left(\sigma \mathscr{F}_{xm}^s - \tilde{x}\mathscr{F}_{\sigma m}^s\right), \quad \mathscr{T}_{\varphi m}^s = \mathscr{F}_{\varphi m}^s,
\end{aligned}\right\} $$
$$(3.14)$$

for $m = 1, 2$, where R is the particle radius.

3.2. *Computation of the force and torque*

The Cartesian components of the force exerted on each particle, P, are given by

$$\left.\begin{aligned}
F_x &= \iint_P f_x \, dS = 2\pi \int_C \mathscr{F}_{x0}\sigma \, dl, \\
F_y &= \iint_P (f_\sigma \cos\varphi - f_\varphi \sin\varphi) \, dS = \pi \int_C \left(\mathscr{F}_{\sigma 1}^c - \mathscr{F}_{\varphi 1}^s\right)\sigma \, dl, \\
F_z &= \iint_P (f_\sigma \sin\varphi + f_\varphi \cos\varphi) \, dS = \pi \int_C \left(\mathscr{F}_{\sigma 1}^s + \mathscr{F}_{\varphi 1}^c\right)\sigma \, dl,
\end{aligned}\right\} \qquad (3.15)$$

where C is the contour of P in a meridional plane, and l is the arclength along C. The Cartesian components of the torque are given by

$$\left.\begin{aligned}
T_x &= \iint_P (\sigma \cos\varphi f_z - \sigma \sin\varphi f_y) \, dS = 2\pi \int_C \mathscr{F}_{\varphi 0}\sigma^2 \, dl, \\
T_y &= \iint_P (\sigma \sin\varphi f_x - \tilde{x} f_z) \, dS = \pi \int_C \left(\sigma \mathscr{F}_{x1}^s - \tilde{x}\mathscr{F}_{\sigma 1}^s - \tilde{x}\mathscr{F}_{\varphi 1}^c\right)\sigma \, dl, \\
T_z &= \iint_P (\tilde{x} f_y - \sigma \cos\varphi f_x) \, dS = \pi \int_C \left(-\sigma \mathscr{F}_{x1}^c + \tilde{x}\mathscr{F}_{\sigma 1}^c - \tilde{x}\mathscr{F}_{\varphi 1}^s\right)\sigma \, dl.
\end{aligned}\right\} \qquad (3.16)$$

It is remarkable that the force and torque depend only on the zeroth and first Fourier coefficients and are independent of the second Fourier coefficients. Referring to (3.8) and (3.9), we see that the zeroth and first coefficients are determined by the particle translational and angular velocities and on the following seven independent components of the traceless matrix $\boldsymbol{M}$,

$$M_{11}, \quad M_{12}, \quad M_{13}, \quad M_{21}, \quad M_{22}, \quad M_{23} - M_{32}, \quad M_{31}. \qquad (3.17)$$

Using the tensor transformation rules, we find that the force and torque in the laboratory frame (X, Y, Z), denoted by the subscript L, are given by

$$\boldsymbol{F}_L = \boldsymbol{A} \cdot \boldsymbol{E}, \qquad \boldsymbol{T}_L = \boldsymbol{A} \cdot \boldsymbol{T}. \qquad (3.18)$$

3.3. *Expansion of the single-layer potential*

The Cartesian components of the single-layer potential take the form

$$\mathscr{S}_j(\boldsymbol{x}_0, \boldsymbol{f}, P) = \iint_P \left[\frac{f_j}{(\hat{x}^2 + \hat{y}^2 + \hat{z}^2)^{1/2}} + \frac{f_x \hat{x} + f_y \hat{y} + f_z \hat{z}}{(\hat{x}^2 + \hat{y}^2 + \hat{z}^2)^{3/2}} (\boldsymbol{x} - \boldsymbol{x}_0)_j \right] dS(\boldsymbol{x})$$

$$= \iint_P \left[\frac{f_j}{\left(\hat{x}^2 + \sigma^2 + \sigma_0^2 - 2\sigma\sigma_0 \cos\hat{\varphi} \right)^{1/2}} \right.$$
$$\left. + \frac{f_x \hat{x} + f_\sigma (\sigma - \sigma_0 \cos\hat{\varphi}) + f_\varphi \sigma_0 \sin\hat{\varphi}}{\left(\hat{x}^2 + \sigma^2 + \sigma_0^2 - 2\sigma\sigma_0 \cos\hat{\varphi} \right)^{3/2}} (\boldsymbol{x} - \boldsymbol{x}_0)_j \right] dS(\boldsymbol{x}), \quad (3.19)$$

where $\hat{\boldsymbol{x}} = \boldsymbol{x} - \boldsymbol{x}_0$. The associated cylindrical polar components are

$$\begin{bmatrix} \mathscr{S}_x \\ \mathscr{S}_\sigma \\ \mathscr{S}_\varphi \end{bmatrix} (\boldsymbol{x}_0, \boldsymbol{f}, P) = \iint_P \frac{1}{\left(\hat{x}^2 + \sigma^2 + \sigma_0^2 - 2\sigma\sigma_0 \cos\hat{\varphi} \right)^{1/2}} \begin{bmatrix} f_x \\ f_\sigma \cos\hat{\varphi} - f_\varphi \sin\hat{\varphi} \\ f_\sigma \sin\hat{\varphi} + f_\varphi \cos\hat{\varphi} \end{bmatrix}$$

$$+ \frac{f_x \hat{x} + f_\sigma (\sigma - \sigma_0 \cos\hat{\varphi}) + f_\varphi \sigma_0 \sin\hat{\varphi}}{\left(\hat{x}^2 + \sigma^2 + \sigma_0^2 - 2\sigma\sigma_0 \cos\hat{\varphi} \right)^{3/2}} \times \begin{bmatrix} \hat{x} \\ \sigma \cos\hat{\varphi} - \sigma_0 \\ \sigma \sin\hat{\varphi} \end{bmatrix} dS(\boldsymbol{x}). \quad (3.20)$$

Substituting (3.11) and simplifying, we find

$$\boldsymbol{S}_\alpha(\boldsymbol{x}_0) = \sum_{m=0}^{2} \int_C \begin{bmatrix} \mathscr{P}_{xxm} \cos(m\varphi_0) & \mathscr{P}_{x\sigma m} \cos(m\varphi_0) & \mathscr{P}_{x\varphi m} \sin(m\varphi_0) \\ \mathscr{P}_{\sigma xm} \cos(m\varphi_0) & \mathscr{P}_{\sigma\sigma m} \cos(m\varphi_0) & \mathscr{P}_{\sigma\varphi m} \sin(m\varphi_0) \\ \mathscr{P}_{\varphi xm} \sin(m\varphi_0) & \mathscr{P}_{\varphi\sigma m} \sin(m\varphi_0) & \mathscr{P}_{\varphi\varphi m} \cos(m\varphi_0) \end{bmatrix} \cdot \begin{bmatrix} \mathscr{F}_{xm}^c \\ \mathscr{F}_{\sigma m}^c \\ \mathscr{F}_{\varphi m}^c \end{bmatrix}$$

$$+ \begin{bmatrix} \mathscr{P}_{xxm} \sin(m\varphi_0) & \mathscr{P}_{x\sigma m} \sin(m\varphi_0) & -\mathscr{P}_{x\varphi m} \cos(m\varphi_0) \\ \mathscr{P}_{\sigma xm} \sin(m\varphi_0) & \mathscr{P}_{\sigma\sigma m} \sin(m\varphi_0) & -\mathscr{P}_{\sigma\varphi m} \cos(m\varphi_0) \\ -\mathscr{P}_{\varphi xm} \cos(m\varphi_0) & -\mathscr{P}_{\varphi\sigma m} \cos(m\varphi_0) & \mathscr{P}_{\varphi\varphi m} \sin(m\varphi_0) \end{bmatrix} \cdot \begin{bmatrix} \mathscr{F}_{xm}^s \\ \mathscr{F}_{\sigma m}^s \\ \mathscr{F}_{\varphi m}^s \end{bmatrix} dl(\boldsymbol{x}). \quad (3.21)$$

The dimensionless single-layer kernels are given by

$$\mathscr{P}_{\alpha\beta 0} = \sigma \begin{bmatrix} \mathscr{I}_{10} + \hat{x}^2 \mathscr{I}_{30} & \hat{x}(\sigma\mathscr{I}_{30} - \sigma_0 \mathscr{I}_{31}) & 0 \\ \hat{x}(\sigma\mathscr{I}_{31} - \sigma_0\mathscr{I}_{30}) & \mathscr{I}_{11} + (\sigma^2 + \sigma_0^2)\mathscr{I}_{31} - \sigma\sigma_0(\mathscr{I}_{32} + \mathscr{I}_{30}) & 0 \\ 0 & 0 & 2\mathscr{I}_{11} \end{bmatrix},$$

$$(3.22)$$

$$\mathscr{P}_{\alpha\beta 1} = \sigma \begin{bmatrix} \mathscr{I}_{11} + \hat{x}^2\mathscr{I}_{31} & \hat{x}(\sigma\mathscr{I}_{31} - \sigma_0\mathscr{I}_{32}) \\ \hat{x}(\sigma\mathscr{I}_{32} - \sigma_0\mathscr{I}_{31}) & \mathscr{I}_{12} + (\sigma^2 + \sigma_0^2)\mathscr{I}_{32} - \sigma\sigma_0(\mathscr{I}_{33} + \mathscr{I}_{31}) \\ \hat{x}\sigma(\mathscr{I}_{32} - \mathscr{I}_{30}) & \mathscr{I}_{12} - \mathscr{I}_{10} + \sigma^2(\mathscr{I}_{32} - \mathscr{I}_{30}) - \sigma\sigma_0(\mathscr{I}_{33} - \mathscr{I}_{31}) \end{bmatrix}$$

$$\begin{matrix} \hat{x}\sigma_0(\mathscr{I}_{32} - \mathscr{I}_{30}) \\ \mathscr{I}_{10} - \mathscr{I}_{12} + \sigma_0^2(\mathscr{I}_{30} - \mathscr{I}_{32}) - \sigma\sigma_0(\mathscr{I}_{31} - \mathscr{I}_{33}) \\ \mathscr{I}_{12} + \sigma\sigma_0(\mathscr{I}_{31} - \mathscr{I}_{33}) \end{matrix} \Bigg],$$

$$(3.23)$$

and

$$\mathscr{P}_{\alpha\beta2} = \sigma \begin{bmatrix} (2\mathscr{I}_{12} - \mathscr{I}_{10}) + \hat{x}^2(2\mathscr{I}_{32} - \mathscr{I}_{30}) \\ \hat{x}\sigma\,(2\mathscr{I}_{33} - \mathscr{I}_{31}) - \hat{x}\sigma_0\,(2\mathscr{I}_{32} - \mathscr{I}_{30}) \\ 2\hat{x}\sigma(\mathscr{I}_{33} - \mathscr{I}_{31}) \end{bmatrix}$$

$$\hat{x}\sigma(2\mathscr{I}_{32} - \mathscr{I}_{30}) - \hat{x}\sigma_0(2\mathscr{I}_{33} - \mathscr{I}_{31})$$
$$2\mathscr{I}_{13} - \mathscr{I}_{11} + (\sigma^2 + \sigma_0^2)(2\mathscr{I}_{33} - \mathscr{I}_{31}) - \sigma\sigma_0\,(2\mathscr{I}_{34} + \mathscr{I}_{32} - \mathscr{I}_{30})$$
$$2(\mathscr{I}_{13} - \mathscr{I}_{11}) + 2\sigma^2(\mathscr{I}_{33} - \mathscr{I}_{31}) - 2\sigma\sigma_0\,(\mathscr{I}_{34} - \mathscr{I}_{32})$$

$$\begin{aligned} & 2\hat{x}\sigma_0(\mathscr{I}_{33} - \mathscr{I}_{31}) \\ 2(\mathscr{I}_{11} - \mathscr{I}_{13}) + 2\sigma_0^2\,(\mathscr{I}_{31} - \mathscr{I}_{33}) - 2\sigma\sigma_0\,(\mathscr{I}_{32} - \mathscr{I}_{34}) \\ (2\mathscr{I}_{13} - \mathscr{I}_{11}) + \sigma\sigma_0\,(-2\mathscr{I}_{34} + 3\mathscr{I}_{32} - \mathscr{I}_{30}) \end{aligned} \Bigg], \quad (3.24)$$

where

$$\mathscr{I}_{mn} \equiv \int_0^{2\pi} \frac{\cos^n\omega\,d\omega}{\left[\hat{x}^2 + \sigma^2 + \sigma_0^2 - 2\sigma\sigma_0\cos\omega\right]^{m/2}} = \frac{4w^m}{(4\sigma\sigma_0)^{m/2}} \int_0^{\pi/2} \frac{(2\cos^2\omega - 1)^n}{(1 - w^2\cos^2\omega)^{m/2}}\,d\omega,$$
$$(3.25)$$

and $w^2 = 4\sigma\sigma_0/[\hat{x}^2 + (\sigma + \sigma_0)^2]$. These integrals can be expressed in terms of complete elliptic integrals of the first or second kind, which are then evaluated either by iterative methods or by standard library functions.

When the point x_0 lies at the surface of a sphere, as $x \to x_0$, $\sigma \to \sigma_0$ and $\theta \to \theta_0$, the diagonal components of the single-layer kernels exhibit logarithmic singularities, where θ is the meridional angle. Detailed consideration reveals

$$\left.\begin{aligned} \mathscr{P}_{xx0} &\sim -2\log|\hat{\theta}|, & \mathscr{P}_{\sigma\sigma0} &\sim -2\log|\hat{\theta}|, & \mathscr{P}_{\varphi\varphi0} &\sim -4\log|\hat{\theta}|, \\ \mathscr{P}_{xx1} &\sim -2\log|\hat{\theta}|, & \mathscr{P}_{\sigma\sigma1} &\sim -2\log|\hat{\theta}|, & \mathscr{P}_{\varphi\varphi1} &\sim -4\log|\hat{\theta}|, \\ \mathscr{P}_{xx2} &\sim -2\log|\hat{\theta}|, & \mathscr{P}_{\sigma\sigma2} &\sim -2\log|\hat{\theta}|, & \mathscr{P}_{\varphi\varphi2} &\sim -3.5\log|\hat{\theta}|, \end{aligned}\right\} \quad (3.26)$$

where $\hat{\theta} = \theta - \theta_0$.

3.4. *Expansion of the double-layer potential*

On the surface of a sphere, the double-layer potential takes the form

$$\begin{aligned} \mathscr{D}_j(x_0, u, P) &= -6 \iint_P \frac{u_x\,\hat{x} + u_y\,\hat{y} + u_z\,\hat{z}}{(\hat{x}^2 + \hat{y}^2 + \hat{z}^2)^{5/2}}(x - x_0)_j(x - x_0)\cdot n(x)\,dS(x) \\ &= -\frac{6}{a} \iint_P \frac{u_x\,\hat{x} + u_\sigma\,(\sigma - \sigma_0\cos\hat{\varphi}) + u_\varphi\,\sigma_0\sin\hat{\varphi}}{(\hat{x}^2 + \sigma^2 + \sigma_0^2 - 2\sigma\sigma_0\cos\hat{\varphi})^{5/2}}(x - x_0)_j\mathscr{G}\,dS(x), \end{aligned}$$
$$(3.27)$$

where $\hat{x} = x - x_0$, and $\mathscr{G} = (x - x_c)\hat{x} + \sigma(\sigma - \sigma_0\cos\hat{\varphi})$. The associated cylindrical polar components are:

$$\begin{bmatrix} \mathscr{D}_x \\ \mathscr{D}_\sigma \\ \mathscr{D}_\varphi \end{bmatrix}(x_0, u, P) = -\frac{6}{a} \iint_P \frac{u_x\hat{x} + u_\sigma\,(\sigma - \sigma_0\cos\hat{\varphi}) + u_\varphi\sigma_0\sin\hat{\varphi}}{(\hat{x}^2 + \sigma^2 + \sigma_0^2 - 2\sigma\sigma_0\cos\hat{\varphi})^{5/2}}$$

$$\times \mathscr{G}\begin{bmatrix} \hat{x} \\ \sigma\cos\hat{\varphi} - \sigma_0 \\ \sigma\sin\hat{\varphi} \end{bmatrix}\,dS(x). \quad (3.28)$$

Substituting (3.10) and simplifying, we find

$$
\mathcal{D}_\alpha(\boldsymbol{x}_0) = \sum_{m=0}^{2} \int_C
\begin{bmatrix}
\mathscr{R}_{xxm}\cos(m\varphi_0) & \mathscr{R}_{x\sigma m}\cos(m\varphi_0) & \mathscr{R}_{x\varphi m}\sin(m\varphi_0) \\
\mathscr{R}_{\sigma xm}\cos(m\varphi_0) & \mathscr{R}_{\sigma\sigma m}\cos(m\varphi_0) & \mathscr{R}_{\sigma\varphi m}\sin(m\varphi_0) \\
\mathscr{R}_{\varphi xm}\sin(m\varphi_0) & \mathscr{R}_{\varphi\sigma m}\sin(m\varphi_0) & \mathscr{R}_{\varphi\varphi m}\cos(m\varphi_0)
\end{bmatrix}
\cdot
\begin{bmatrix}
\mathscr{U}_{xm}^c \\ \mathscr{U}_{\sigma m}^c \\ \mathscr{U}_{\varphi m}^c
\end{bmatrix}
$$
$$
+
\begin{bmatrix}
\mathscr{R}_{xxm}\sin(m\varphi_0) & \mathscr{R}_{x\sigma m}\sin(m\varphi_0) & -\mathscr{R}_{x\varphi m}\cos(m\varphi_0) \\
\mathscr{R}_{\sigma xm}\sin(m\varphi_0) & \mathscr{R}_{\sigma\sigma m}\sin(m\varphi_0) & -\mathscr{R}_{\sigma\varphi m}\cos(m\varphi_0) \\
-\mathscr{R}_{\varphi xm}\cos(m\varphi_0) & -\mathscr{R}_{\varphi\sigma m}\cos(m\varphi_0) & \mathscr{R}_{\varphi\varphi m}\sin(m\varphi_0)
\end{bmatrix}
\cdot
\begin{bmatrix}
\mathscr{U}_{xm}^s \\ \mathscr{U}_{\sigma m}^s \\ \mathscr{U}_{\varphi m}^s
\end{bmatrix}
\, \mathrm{d}l(\boldsymbol{x}).
\tag{3.29}
$$

The double-layer kernels are given by

$$
\mathscr{R}_{\alpha\beta 0} = -\frac{6\sigma}{a}
\begin{bmatrix}
\tau\hat{x}^2\mathscr{I}_{50} - \sigma\sigma_0\hat{x}^2\mathscr{I}_{51} \\
\tau\hat{x}(\sigma\mathscr{I}_{51}-\sigma_0\mathscr{I}_{50}) - \sigma\sigma_0\hat{x}(\sigma\mathscr{I}_{52}-\sigma_0\mathscr{I}_{51}) \\
0
\end{bmatrix}
$$
$$
\begin{matrix}
\tau\hat{x}(\sigma\mathscr{I}_{50}-\sigma_0\mathscr{I}_{51}) - \sigma\sigma_0\hat{x}(\sigma\mathscr{I}_{51}-\sigma_0\mathscr{I}_{52}) \\
(\tau\sigma^2+\tau\sigma_0^2+\sigma^2\sigma_0^2)\mathscr{I}_{51} - \sigma\sigma_0(\tau+\sigma^2+\sigma_0^2)\mathscr{I}_{52} + \sigma^2\sigma_0^2\mathscr{I}_{53} - \tau\sigma\sigma_0\mathscr{I}_{50} \\
0
\end{matrix}
$$
$$
\left.
\begin{matrix}
0 \\
0 \\
\tau\sigma\sigma_0(\mathscr{I}_{50}-\mathscr{I}_{52}) - \sigma^2\sigma_0^2(\mathscr{I}_{51}-\mathscr{I}_{53})
\end{matrix}
\right],
\tag{3.30}
$$

$$
\mathscr{R}_{\alpha x1} = -\frac{6\sigma}{a}
\begin{bmatrix}
\tau\hat{x}^2\mathscr{I}_{51} - \sigma\sigma_0\hat{x}^2\mathscr{I}_{52} \\
\tau\hat{x}(\sigma\mathscr{I}_{52}-\sigma_0\mathscr{I}_{51}) - \sigma\sigma_0\hat{x}(\sigma\mathscr{I}_{53}-\sigma_0\mathscr{I}_{52}) \\
\tau\hat{x}\sigma(\mathscr{I}_{52}-\mathscr{I}_{50}) - \sigma^2\sigma_0\hat{x}(\mathscr{I}_{53}-\mathscr{I}_{51})
\end{bmatrix}
$$
$$
\begin{matrix}
\tau\hat{x}(\sigma\mathscr{I}_{51}-\sigma_0\mathscr{I}_{52}) - \sigma\sigma_0\hat{x}(\sigma\mathscr{I}_{52}-\sigma_0\mathscr{I}_{53}) \\
\tau(\sigma^2+\sigma_0^2)\mathscr{I}_{52} - \tau\sigma\sigma_0(\mathscr{I}_{53}+\mathscr{I}_{51}) - \sigma\sigma_0(\sigma^2+\sigma_0^2)\mathscr{I}_{53} + \sigma^2\sigma_0^2(\mathscr{I}_{54}+\mathscr{I}_{52}) \\
\tau\sigma^2(\mathscr{I}_{52}-\mathscr{I}_{50}) - \tau\sigma\sigma_0(\mathscr{I}_{53}-\mathscr{I}_{51}) - \sigma^3\sigma_0(\mathscr{I}_{53}-\mathscr{I}_{51}) + \sigma^2\sigma_0^2(\mathscr{I}_{54}-\mathscr{I}_{52})
\end{matrix}
$$
$$
\left.
\begin{matrix}
\tau\hat{x}\sigma_0(\mathscr{I}_{52}-\mathscr{I}_{50}) - \sigma\sigma_0^2\hat{x}(\mathscr{I}_{53}-\mathscr{I}_{51}) \\
\tau\sigma_0^2(\mathscr{I}_{50}-\mathscr{I}_{52}) - \tau\sigma\sigma_0(\mathscr{I}_{51}-\mathscr{I}_{53}) - \sigma\sigma_0^3(\mathscr{I}_{51}-\mathscr{I}_{53}) + \sigma^2\sigma_0^2(\mathscr{I}_{52}-\mathscr{I}_{54}) \\
\tau\sigma\sigma_0(\mathscr{I}_{51}-\mathscr{I}_{53}) - \sigma^2\sigma_0^2(\mathscr{I}_{52}-\mathscr{I}_{54})
\end{matrix}
\right],
\tag{3.31}
$$

and

$$
\mathscr{R}_{\alpha x2} = -\frac{6\sigma}{a}
\begin{bmatrix}
\tau\hat{x}^2(2\mathscr{I}_{52}-\mathscr{I}_{50}) - \sigma\sigma_0\hat{x}^2(2\mathscr{I}_{53}-\mathscr{I}_{51}) \\
\tau\hat{x}\sigma(2\mathscr{I}_{53}-\mathscr{I}_{51}) - \tau\hat{x}\sigma_0(2\mathscr{I}_{52}-\mathscr{I}_{50}) - \hat{x}\sigma^2\sigma_0(2\mathscr{I}_{54}-\mathscr{I}_{52}) \\
\quad +\hat{x}\sigma\sigma_0^2(2\mathscr{I}_{53}-\mathscr{I}_{51}) \\
2\tau\hat{x}\sigma(\mathscr{I}_{53}-\mathscr{I}_{51}) - 2\hat{x}\sigma^2\sigma_0(\mathscr{I}_{54}-\mathscr{I}_{52})
\end{bmatrix}
$$
$$
\begin{matrix}
\tau\hat{x}\sigma(2\mathscr{I}_{52}-\mathscr{I}_{50}) - \tau\hat{x}\sigma_0(2\mathscr{I}_{53}-\mathscr{I}_{51}) - \sigma^2\sigma_0\hat{x}(2\mathscr{I}_{53}-\mathscr{I}_{51}) + \sigma\sigma_0^2\hat{x}(2\mathscr{I}_{54}-\mathscr{I}_{52}) \\
\tau(\sigma^2+\sigma_0^2)(2\mathscr{I}_{53}-\mathscr{I}_{51}) - \tau\sigma\sigma_0(2\mathscr{I}_{54}+\mathscr{I}_{52}-\mathscr{I}_{50}) \\
\quad -\sigma\sigma_0(\sigma^2+\sigma_0^2)(2\mathscr{I}_{54}-\mathscr{I}_{52}) + \sigma^2\sigma_0^2(2\mathscr{I}_{55}+\mathscr{I}_{53}-\mathscr{I}_{51}) \\
2\tau\sigma^2(\mathscr{I}_{53}-\mathscr{I}_{51}) - 2\tau\sigma\sigma_0(\mathscr{I}_{54}-\mathscr{I}_{52}) - 2\sigma^3\sigma_0(\mathscr{I}_{54}-\mathscr{I}_{52}) + 2\sigma^2\sigma_0^2(\mathscr{I}_{55}-\mathscr{I}_{53})
\end{matrix}
$$
$$
\left.
\begin{matrix}
2\tau\hat{x}\sigma_0(\mathscr{I}_{53}-\mathscr{I}_{51}) - 2\sigma\sigma_0^2\hat{x}(\mathscr{I}_{54}-\mathscr{I}_{52}) \\
2\tau\sigma_0^2(\mathscr{I}_{51}-\mathscr{I}_{53}) - 2\tau\sigma\sigma_0(\mathscr{I}_{52}-\mathscr{I}_{54}) - 2\sigma\sigma_0^3(\mathscr{I}_{52}-\mathscr{I}_{54}) + 2\sigma^2\sigma_0^2(\mathscr{I}_{53}-\mathscr{I}_{55}) \\
\tau\sigma\sigma_0(-2\mathscr{I}_{54}+3\mathscr{I}_{52}-\mathscr{I}_{50}) - \sigma^2\sigma_0^2(-2\mathscr{I}_{55}+3\mathscr{I}_{53}-\mathscr{I}_{51})
\end{matrix}
\right],
\tag{3.32}
$$

where $\tau = \hat{x}\tilde{x} + \sigma^2$ and $\tilde{x} = x - x_c$.

When the point x_0 lies at the surface of a sphere, the components of the double-layer kernels exhibiting singular behaviour are

$$\mathscr{R}_{\varphi\varphi 0} \sim \frac{6}{R} \log |\hat{\theta}|, \qquad \mathscr{R}_{\varphi\varphi 1} \sim \frac{5.5}{R} \log |\hat{\theta}|, \qquad \mathscr{R}_{\varphi\varphi 2} \sim \frac{5}{R} \log |\hat{\theta}|, \qquad (3.33)$$

where R is the sphere radius. All other entries exhibit a regular behaviour. These logarithmic singularities are consistent with the following ordering of principal-value integrals for the double-layer potential in Stokes flow: the integrand of two-dimensional flow is discontinuous along the boundary contour at the singular point; the integrand of axisymmetric flow corresponding to a Fourier expansion is logarithmically singular along the trace of the boundary in a meridional plane; and the integrand of three-dimensional flow exhibits an integrable, simple pole $(1/r)$ singularity over a locally curved surface.

4. Integral equations

Substituting the Fourier expansions into the integral equation (3.7) and collecting the Fourier coefficients, we derive three decoupled systems of integral equations that can be solved separately in isolation. For $m = 0$, we find

$$\int_C \mathscr{P}_{\alpha\beta 0} \mathscr{F}_{\beta 0} \, \mathrm{d}l - \mu \int_C \mathscr{R}_{\alpha\beta 0} \mathscr{U}^S_{\beta 0} \, \mathrm{d}l + 4\pi\mu \mathscr{U}^S_{\alpha 0} = -8\pi\mu \big(\mathscr{U}^{RBM}_{\alpha 0} - \mathscr{U}^{\infty}_{\alpha 0}\big). \qquad (4.1)$$

Inspecting the kernels, we find that this system can be further decomposed into a first subsystem of two integral equations for the axial and radial components of the traction, and a second subsystem of one integral equation for the meridional component of the traction. In the case of the mobility problem, the first subsystem is used to compute the x-component of the particle translational velocity for a specified x-component of the force, and the second subsystem is used to compute the x-component of the particle angular velocity for a specified x-component of the torque. For $m = 1, 2$, we find

$$\int_C \big[\mathscr{P}^{cc}_{\alpha\beta m} \mathscr{F}^c_{\beta m} - \mathscr{P}^{cs}_{\alpha\beta m} \mathscr{F}^s_{\beta m}\big] \, \mathrm{d}l - \mu \int_C \big[\mathscr{R}^{cc}_{\alpha\beta m} \mathscr{U}^{c^S}_{\beta m} - \mathscr{R}^{cs}_{\alpha\beta m} \mathscr{U}^{s^S}_{\beta m}\big] \, \mathrm{d}l + 4\pi\mu \mathscr{U}^{c^S}_{\alpha m}$$
$$= -8\pi\mu \big(\mathscr{U}^{c^{RBM}}_{\alpha m} - \mathscr{U}^{c^{\infty}}_{\alpha m}\big), \quad (4.2)$$

and

$$\int_C \big[\mathscr{P}^{sc}_{\alpha\beta m} \mathscr{F}^c_{\beta m} + \mathscr{P}^{ss}_{\alpha\beta m} \mathscr{F}^s_{\beta m}\big] \, \mathrm{d}l - \mu \int_C \big[\mathscr{R}^{sc}_{\alpha\beta m} \mathscr{U}^{c^S}_{\beta m} + \mathscr{R}^{ss}_{\alpha\beta m} \mathscr{U}^{s^S}_{\beta m}\big] \, \mathrm{d}l + 4\pi\mu \mathscr{U}^{s^S}_{\alpha m}$$
$$= -8\pi\mu \big(\mathscr{U}^{s^{RBM}}_{\alpha m} - \mathscr{U}^{s^{\infty}}_{\alpha m}\big), \quad (4.3)$$

where the shown complementary kernels are defined as

$$\mathscr{P}^{cc}_{\alpha\beta m} = \mathscr{P}^{ss}_{\alpha\beta m} = \begin{bmatrix} \mathscr{P}_{xxm} & \mathscr{P}_{x\sigma m} & 0 \\ \mathscr{P}_{\sigma xm} & \mathscr{P}_{\sigma\sigma m} & 0 \\ 0 & 0 & \mathscr{P}_{\varphi\varphi m} \end{bmatrix}, \qquad (4.4a)$$

$$\mathscr{P}^{cs}_{\alpha\beta m} = \mathscr{P}^{sc}_{\alpha\beta m} = \begin{bmatrix} 0 & 0 & \mathscr{P}_{x\varphi m} \\ 0 & 0 & \mathscr{P}_{\sigma\varphi m} \\ \mathscr{P}_{\varphi xm} & \mathscr{P}_{\varphi\sigma m} & 0 \end{bmatrix}. \qquad (4.4b)$$

The double-layer kernels arise by replacing $\mathscr{P}$ with $\mathscr{R}$ in these expressions. In the case of the mobility problem, the system for $m = 1$ is used to compute the y and z components of the translational and angular velocities from corresponding specified components of the force and torque. We emphasize again that solving the system for $m = 2$ is not required for the computation of the force and torque in the resistance problem or for the computation of the particle velocities in the mobility problem.

An integral identity states that $S(x_0, n, P) = 0$, where P is the surface of each sphere, reflecting the indeterminacy of the pressure. Accordingly,

$$\int_C \mathscr{P}_{\alpha\beta0} n_\beta \, \mathrm{d}l = 0, \tag{4.5}$$

and the integral equation for the zeroth-order Fourier terms does not have a unique solution, where C the contour of each sphere in a meridional plane. To remove the eigenfunction, we deflate the spectrum of the single-layer potential by adding to the left-hand side of (4.1) the term

$$n_\alpha(x_0) \int_C n_\beta(x) \mathscr{F}_{\beta0}(x) \, \mathrm{d}l(x). \tag{4.6}$$

This modification ensures a perfectly well-posed problem.

5. Stresslet and particle stress tensor

In the case of force-free and torque-free particles, the flow far from the particles is induced by a stresslet with strength

$$s_{ij} = \frac{1}{2} \iint_P [x_i \, f_j + x_j \, f_i - 2\mu(u_i n_j + u_j n_i)] \, \mathrm{d}S, \tag{5.1}$$

where the integration is performed over the surfaces of both particles (e.g. Pozrikidis 1992, p. 48). Note that the integral remains unchanged when the origin is shifted to a new location. When the boundary conditions over the particle surfaces express rigid-body motion, the integral involving the velocity is zero, and the stresslet depends only on the particle traction. In our case, because of the slip velocity, the velocity term makes a finite contribution. Substituting the Maxwell–Basset boundary condition and simplifying, we find

$$s_{ij} = \frac{1}{2} \iint_P [x_i \, f_j + x_j \, f_i - \frac{2L}{\beta}(f_i^| n_j + f_j^| n_i)] \, \mathrm{d}S, \tag{5.2}$$

where $f_i^|$ is the tangential component of the traction, $f^| = n \times f \times n = f \cdot (I - nn)$. For a spherical particle of radius R,

$$s_{ij} = \mathscr{I}_{ij}(f) - \frac{2L}{\beta R} \mathscr{I}_{ij}(f^|), \tag{5.3}$$

where

$$\mathscr{I}_{ij}(f) = \frac{1}{2} \iint_P [\tilde{x}_i \, f_j + \tilde{x}_j \, f_i] \, \mathrm{d}S, \tag{5.4}$$

and $\tilde{x} = x - x_c$. Substituting the Fourier expansions and performing the integration in the meridional direction, we derive expressions in terms of contour integrals,

$$
\left.
\begin{aligned}
\mathscr{I}_{xx}(f) &= 2\pi \int_C \mathscr{F}_{x0}\sigma\tilde{x}\,\mathrm{d}l, \quad \mathscr{I}_{xy}(f) = \frac{\pi}{2}\int_C \left[\tilde{x}\left(\mathscr{F}_{\sigma 1}^c - \mathscr{F}_{\varphi 1}^s\right) + \sigma\mathscr{F}_{x1}^c\right]\sigma\,\mathrm{d}l, \\
\mathscr{I}_{xz}(f) &= \frac{\pi}{2}\int_C \left[\tilde{x}\left(\mathscr{F}_{\sigma 1}^s + \mathscr{F}_{\varphi 1}^c\right) + \sigma\mathscr{F}_{x1}^s\right]\sigma\,\mathrm{d}l, \\
\mathscr{I}_{yy}(f) &= \pi \int_C \left(\mathscr{F}_{\sigma 0} + \frac{1}{2}\mathscr{F}_{\sigma 2}^c - \frac{1}{2}\mathscr{F}_{\varphi 2}^s\right)\sigma^2\,\mathrm{d}l, \quad \mathscr{I}_{yz}(f) = \frac{\pi}{2}\int_C \left(\mathscr{F}_{\varphi 2}^c + \mathscr{F}_{\sigma 2}^s\right)\sigma^2\,\mathrm{d}l, \\
\mathscr{I}_{zz}(f) &= \pi \int_C \left(\mathscr{F}_{\sigma 0} - \frac{1}{2}\mathscr{F}_{\sigma 2}^c + \frac{1}{2}\mathscr{F}_{\varphi 2}^s\right)\sigma^2\,\mathrm{d}l.
\end{aligned}
\right\}
$$

(5.5)

Replacing $\mathscr{F}$ with $\mathscr{T}$ we obtain corresponding expressions for $\mathscr{I}_{ij}(f^{\mid})$. These expressions reveal that the off-diagonal components of the stresslet depend on the zeroth and first Fourier coefficients, while the diagonal components depend on the zeroth, first and second Fourier coefficients.

Using the rules of tensor transformation, we find that the stresslet in the laboratory frame is given by

$$
S = A \cdot s \cdot A^T.
$$

(5.6)

The dimensionless particle stress tensor is defined as

$$
\Sigma = \frac{3}{4\pi a^3(1 + \delta^3)\mu k}S,
$$

(5.7)

where k is an appropriate constant shear or extensional rate.

6. Numerical methods

To solve the integral equations derived in §4, we divide the particle contours in the $\varphi = 0$ meridional plane into circular elements, and approximate the Fourier coefficients with constant functions over each element. For best accuracy, the elements are concentrated near the axis of symmetry so that their length increases geometrically with distance from the axis of symmetry. Given the number of elements, the element stretch ratio is determined by r-adaptation, so that the size of the element in the middle of the inter-particle gap is comparable to the gap size (figure 2.) The integrals over the boundary elements are computed using the six-point Gauss–Legendre quadrature. The logarithmic singularities of the singular elements are subtracted off and computed analytically over the circular segments.

Now applying point collocation at the midpoint of each element, we generate a system of linear equations for the unknown solution vectors consisting of the particle-element traction. In the case of freely suspended particles, the unknown translational and angular velocities are appended to the vector of unknowns for the zeroth and first Fourier coefficients. Specifically, the x-velocity is appended to the first zeroth-order subsystem, and the x angular velocity is appended to the second zeroth-order subsystem. The rest of the unknowns are appended to the first-order system. Twelve more equations are then apportioned to ensure the vanishing of the Cartesian components of the force and torque over each particle.

Equations (2.20) governing the particle motion are integrated in time using the second-order Runge–Kutta method. When the particle gap is small, large lubrication forces develop rendering the differential equations stiff and raising the possibility of
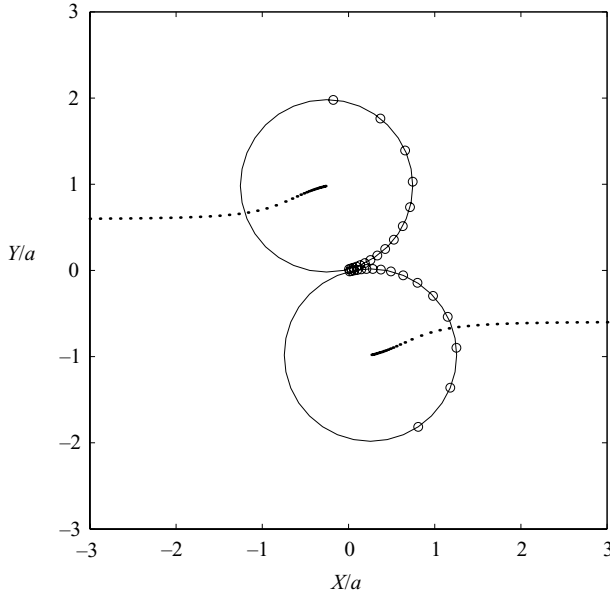
FIGURE 2. Adaptive distribution of collocation points on two intercepting spheres according to the particle gap. The dotted lines trace the particle centre trajectories.

unnatural collision and artificial overlap at a finite time. Overlap is tolerated in other Stokesian dynamics simulations, but is deemed unacceptable in our approach. To ensure a regular behaviour, the time step is adjusted according to the particle gap, ϵ, and the relative particle velocity in the laboratory frame, as $\Delta t = \omega \epsilon / |\boldsymbol{V}^A - \boldsymbol{V}^B|$, where ω is a numerical coefficient. This time step is accepted only if it is lower than a specified value, Δt_0, used for well-separated particles. Numerical experimentation showed that this adaptive protocol yields the best results compared to other similar protocols explored. The numerical method was implemented in a MATLAB code with embedded animation. A complete simulation requires a few dozen to several hundred time steps and consumes a few hours to a few days of CPU time on 2.0 GHz desktop Linux computer.

To assess the performance of the numerical method, we consider the interception of two equal spheres whose centres are initially located at $\boldsymbol{X}_A/a = (0.6, -3, 0)$, and $\boldsymbol{X}_B/a = (-0.6, 3, 0)$. Figure 2 shows the early part of the particle trajectories in the absence of slip velocity and demonstrates that the spheres come into near-physical contact, although they never collide. Figure 3(a) compares the trajectory of the centre of sphere A, computed using analytical expressions for the particle velocity given in the Appendix (dotted lines), with that computed using the boundary element method using sixty-four elements, $k\Delta t_0 = 0.20$, and $\omega = 1.0$ (dashed line). The agreement is exceptional, as the upper dotted line and solid line are indistinguishable. Close inspection reveals that the differences in the particle centre position are on the order of $10^{-5}a$ throughout and upon completion of the interception. Figure 3(b) describes the evolution of the time step for the simulation presented in figure 3(a), and demonstrates a drastic reduction by one order of magnitude in the near-contact regime.

Figure 3(c) shows the evolution of the minimum gap between the intercepting spheres computed with 128 elements, $k\Delta t_0 = 0.20$, and $\omega = 1.0$. We observe a drastic reduction by nearly two orders of magnitude as the particles undergo a near-collision.
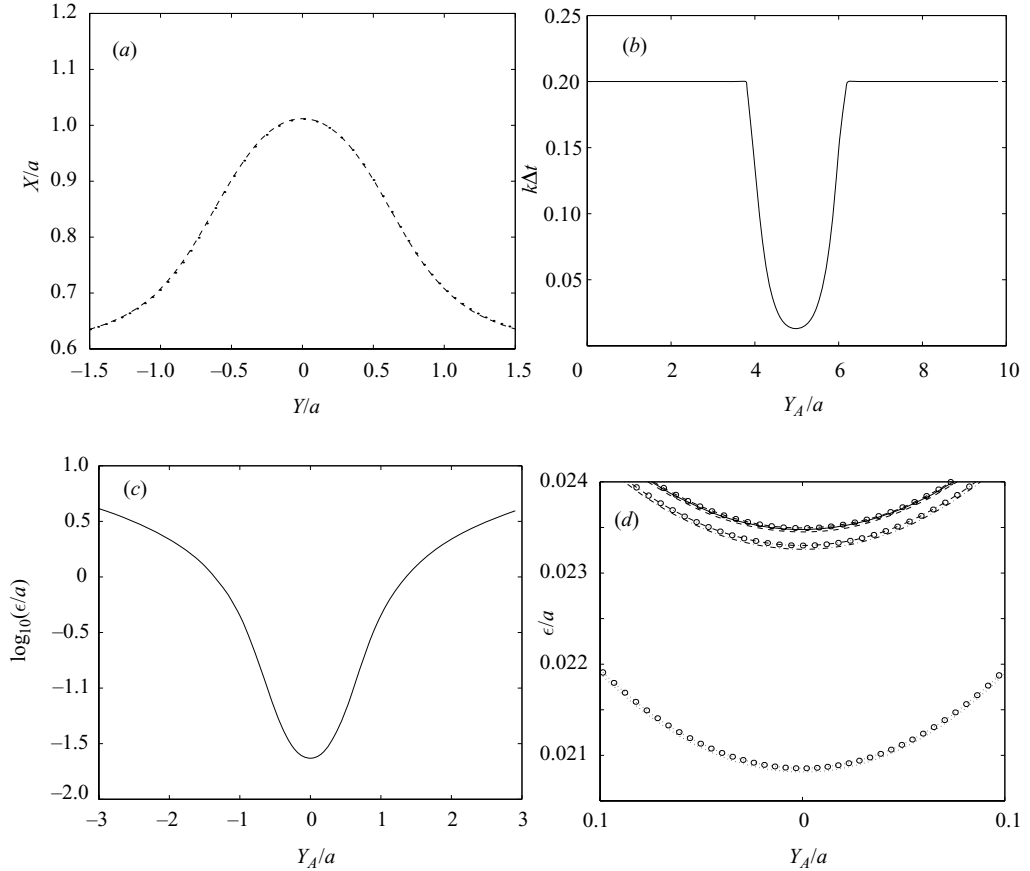
FIGURE 3. (a) Particle centre trajectories in the XY plane (dashed line) are compared with those computed using analytical expressions for the particle velocity (dotted lines), for initial particle positions $X_A/a = (0.6, -3, 0)$ and $X_B/a = (-0.6, 3, 0)$, and no-slip surfaces. (b) Adaptive evolution of the time step according to the inter-particle gap. (c) Evolution of the gap between the two intercepting particles plotted on a semi-logarithmic scale. (d) Evolution of the gap between the two intercepting particles; the dotted, dot-dashed, dashed, and solid lines correspond to simulations conducted, respectively, with 16, 32, 64, and 128 boundary elements, $k\Delta t_0 = 0.20$, and $\omega = 1.0$; the curves traced by the symbols duplicate the results with $\omega = 0.5$.

The minimum separation occurring in the vertical orientation along the X-axis is on the order of $10^{-2}a$. The accuracy and convergence of the numerical method are tested in figure 3(d), where the minimum gap is plotted against the particle centre longitudinal position. The lowest dotted, dot-dashed, dashed, and solid lines correspond to simulations conducted, respectively, with 16, 32, 64, and 128 boundary elements, using $k\Delta t_0 = 0.20$, and $\omega = 1.0$. The curves with the circular symbols duplicate the simulations with a smaller time step, $\omega = 0.5$. The results converge smoothly and fast as the number of boundary elements is doubled.

Further computations with one particle subject to the slip boundary condition confirmed that the numerical results are in excellent agreement with an analytical solution based on the singularity method (Luo & Pozrikidis 2007). The numerical error in the simulation of two particles is comparable to that discussed in this section for no-slip surfaces.
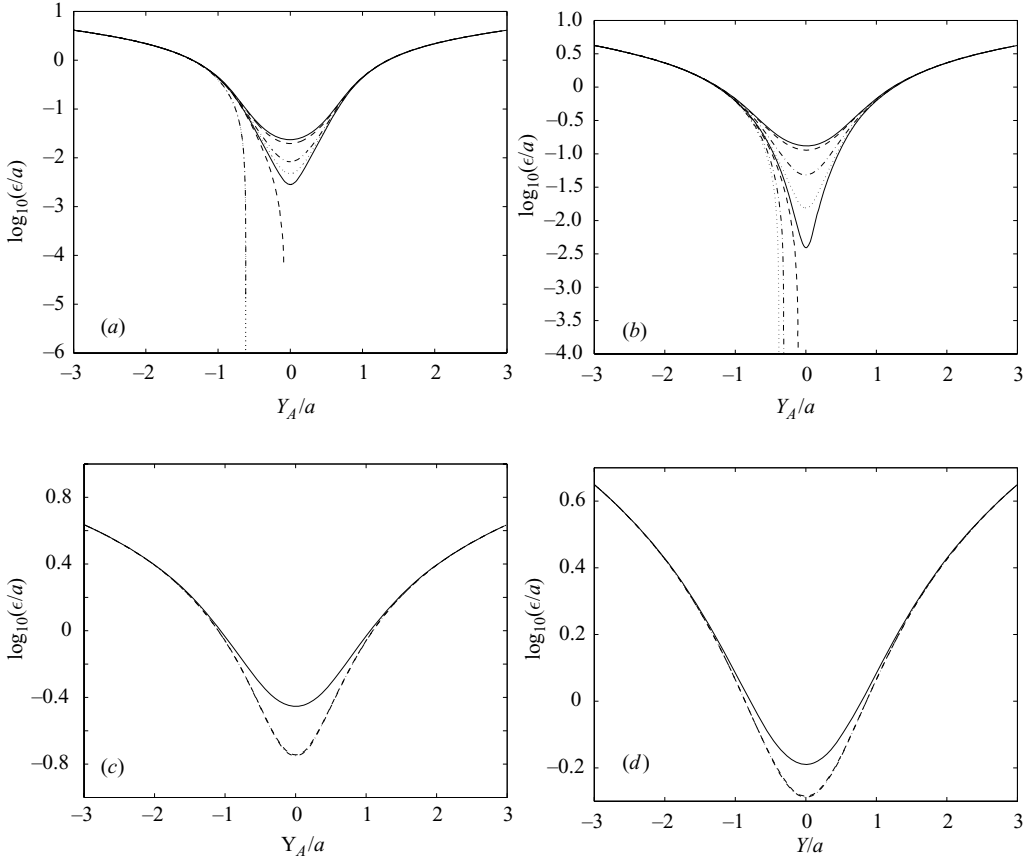
FIGURE 4. Effect of the surface slip on the evolution of the minimum gap between two spheres intercepting in the (X, Y) plane, starting from the longitudinal position $Y_A/a = -3$. (*a*) Initial height $X_A/a = 0.6$ and $\beta_p = \infty$ (upper solid line), 500 (dashed line), 100 (dot-dashed line), 75 (dotted line), 65 (solid line), 50 (dot-dashed line); and 5 (dashed line for 64 elements, dotted line for 128 elements). (*b*) Initial height $X_A/a = 0.8$ and $\beta_p = \infty$ (upper solid line), 75 (dashed line), 10 (dot-dashed line), 5 (dotted line), 3.75 (solid line), 3 (dashed line), 1.0 (dot-dashed line), and 0.1 (lower dotted line). (*c*) $X_A/a = 1.0$ and $\beta_p = \infty$ (solid line) 0.1 (dashed line), and 0 (dot-dashed line). (*d*) $X_A/a = 1.2$ and $\beta_p = \infty$ (solid line), 0.1 (dashed line), and 0.0 (dot-dashed line).

7. Particle interception in simple shear flow

Our main objective is to investigate the effect of the surface slip on the particle trajectories and rheology of dilute suspensions. Several series of simulations were conducted for force-free and torque-free particles of equal size convected in a simple shear flow described by equations (2.10). Unless otherwise specified, the contour of each particle is discretized into sixty-four elements, the particle centre trajectories lie in the (X, Y) plane, $Z_A = Z_B = 0$, and the origin is set such that $Y_B = -Y_A$ throughout the motion.

7.1. *Particle trajectories*

Figure 4 describes the evolution of the gap between two particles approaching from infinity and starting from several initial positions along the X-axis. In these graphs, the logarithm of the gap is plotted against the longitudinal position of the first particle,
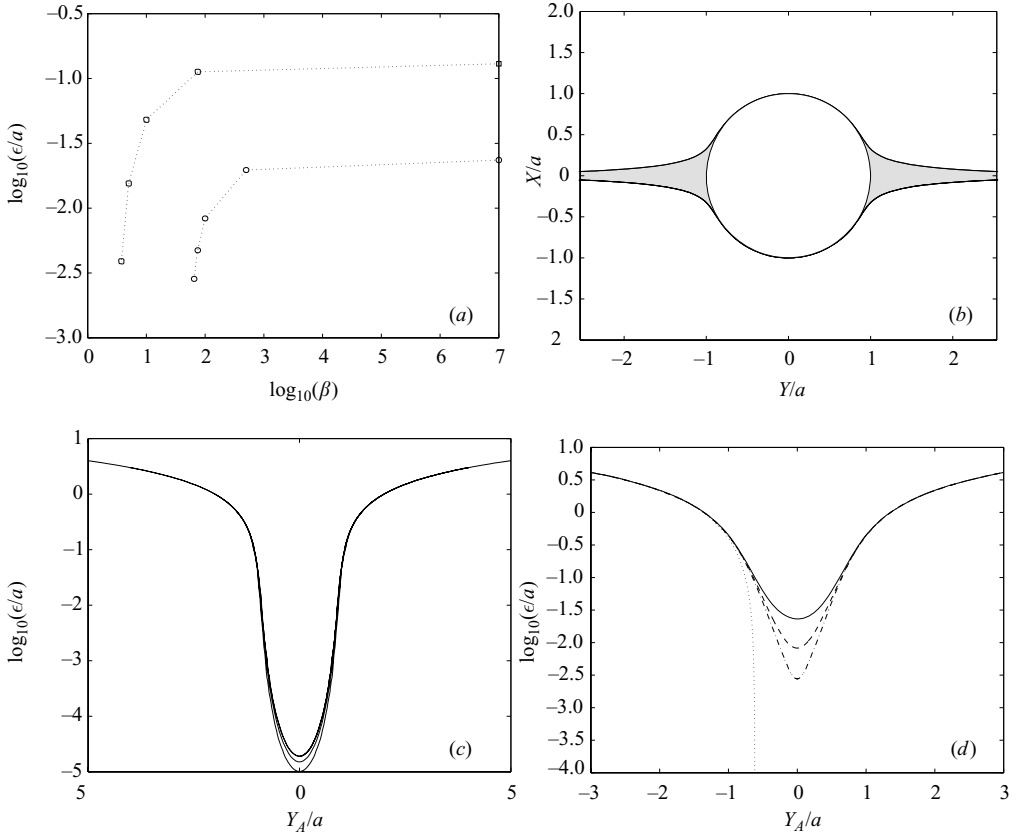
FIGURE 5. (*a*) Effect of surface slip on the minimum gap between two spheres intercepting in the (X, Y)-plane for initial longitudinal position $Y_A/a = -3$ and $X_A/a = 0.6$ (circles) or 0.8 (squares). (*b*) Initial particle centre positions in the (X, Y)-plane inside the shaded area lead to closed particle trajectories for no-slip surfaces; the evolution of the minimum gap for particles initially located on the Y-axis is shown in (*c*). (*d*) Effect of the surface slip on the evolution of the minimum gap between two spheres intercepting off the (X, Y)-plane starting from the initial position $X_A/a = 0.6/\sqrt{2}$, $Y_A/a = -3$, and $Z_A/a = 0.6/\sqrt{2}$, for $\beta_p = \infty$ (solid line), 100 (dashed line), 65 (dot-dashed line), 5 (dotted line).

Y_A. For each initial position, results are presented for several values of the slip coefficient β including the limiting value of infinity corresponding to no-slip surfaces. In all cases, when the slip coefficient is sufficiently large, the particles roll over one another and separate after reaching a minimum gap in the vertical orientation along the X-axis, occurring at $Y_A = 0$.

The numerical results strongly suggest the existence of a critical value of the slip coefficient for sufficiently small initial separations along the X-axis, below which the particles come into physical contact at some point during the interception. The critical value of the slip coefficient depends on the relative initial particle positions. The evidence is best illustrated in figure 5(*a*), showing a graph of the minimum gap during the interception plotted against the slip coefficient on a log-log scale. Since a contact force is not implemented in the mathematical model, nothing prevents two colliding particles from penetrating one another, causing the numerical method

to fail. In practice, the calculations with sixty-four boundary elements around each particle cease to be reliable when the minimum gap between the particles becomes on the order of $10^{-5}a$. Figure 4(a) shows the results of a duplicate calculation with 128 elements for $\beta = 5$, conducted to confirm the accuracy of the cruder computation and further demonstrate the rapid decline of the gap.

In reality, once the particles come in contact, attraction and adhesion forces will cause the formation of a transient or permanent dipole. Depending on the strength of the adhesion forces, the doublet may separate when its axis has been aligned with the principal axis of stretching of the simple shear flow, which is inclined by an angle of $\pi/4$ with respect to the y-axis. In principle, we can identify the collision time, continue the simulation with two attached particles, and allow the particles to be detached when the relative particle velocity points away from the line connecting their centres. However, it would be necessary also to state whether the touching particles can roll over one another while attached, and this raises the possible modes of motion.

Batchelor & Green (1972a) pointed out that not all trajectories originate from infinity, as illustrated in figure 5(b) for no-slip surfaces. Initial particle centre positions symmetrically located with respect to the origin inside the shaded area lead to closed trajectories with the particles exhibiting a perpetual orbiting motion. When the particles are initially located on the Y-axis, they migrate off the axis and nearly touch when they reach the vertical orientation along the X-axis. The evolution of the minimum gap for particles initially located on the Y-axis is shown in figure 5(c). These particle trajectories were computed using the analytical expressions for the velocity given in the Appendix. An inflection point is observed when the gap is on the order of $10^{-3}a$ in all cases, and the graphs subsequently become upward concave. Unfortunately, we are unable to simulate these periodic orbits as the inter-particle gap becomes prohibitively small at some point during the motion, and the simulations with sixty-four elements are not reliable in their entire length. However, based on our results for open trajectories, we expect that allowing for slip will lead to collision even at relatively high values of the slip coefficient.

Similar behaviour is observed for particles intercepting off the (X, Y)-plane, as shown in figure 5(d). As the slip coefficient decreases, the minimum gap becomes smaller and tends to zero at a certain point during the interception.

7.2. *Particle stress tensor*

Batchelor (1970) showed that the effective stress tensor of a suspension of force-free spherical particles freely convected in an infinite linear flow is given by

$$\boldsymbol{\sigma}_{\text{Eff}} = \mu\left(2\boldsymbol{E}^{\infty} + \frac{1}{V}\boldsymbol{s}\right), \tag{7.1}$$

where $\boldsymbol{E}^{\infty}$ is the rate-of-deformation tensor of the linear flow, and $\boldsymbol{s}$ is the stresslet computed over the surfaces of all particles in a given volume, V. In the limit of infinite dilution, $\boldsymbol{s} \simeq n\boldsymbol{s}^{(1)}$, where $\boldsymbol{s}^{(1)}$ is the stresslet computed over the surface of one particle, and n is the particle number density defined as the number of particles in the given volume V, divided by V. Thus,

$$\boldsymbol{\sigma}_{\text{Eff}} \simeq \mu\left(2\boldsymbol{E}^{\infty} + \frac{n}{V}\boldsymbol{s}^{(1)}\right) \equiv \mu\left(2\boldsymbol{E}^{\infty} + ck\boldsymbol{\Sigma}^{(1)}\right), \tag{7.2}$$

where $c = nV_p$ is the particle volume fraction,

$$\boldsymbol{\Sigma}^{(1)} \equiv \frac{1}{kV_p}\boldsymbol{s}^{(1)} \tag{7.3}$$

is the one-particle stress tensor, V_p is the volume of one particle, and k is a properly defined shear or elongational rate. A detailed calculation shows that

$$\boldsymbol{\Sigma}^{(1)} = \frac{2\alpha_1}{k} \boldsymbol{E}^{\infty}, \tag{7.4}$$

and thus

$$\boldsymbol{\sigma}_{\mathrm{Eff}} \simeq \mu(1 + \alpha_1 c) 2 \boldsymbol{E}^{\infty}, \tag{7.5}$$

where α_1 is a constant. A dilute suspension of spherical particle thus behaves like a Newtonian fluid with increased viscosity.

For rigid particles with no-slip surfaces, Einstein (1906) calculated $\alpha_1 = 5/2$. For spherical drops enclosing a fluid with viscosity $\lambda\mu$, Taylor (1932) calculated

$$\alpha_1 = \frac{1}{2} \frac{5\lambda + 2}{\lambda + 1}. \tag{7.6}$$

The Einstein value arises in the limit $\lambda \to \infty$. Luo & Pozrikidis (2007) derived an exact singularity solution for infinite linear flow past a spherical particle with a slip surface and found

$$\alpha_1 = \frac{5}{2} \frac{\beta + 2}{\beta + 5}. \tag{7.7}$$

As the slip coefficient β decreases from infinity to zero, the particle stress tensor of an infinite dilute suspension decreases from the Einstein value of $5/2$ to the value of unity. Comparing (7.7) to (7.6), we see that the slip coefficient, β, is the counterpart of the viscosity ratio, λ.

The rate-of-deformation tensor of the one-particle suspension can be expressed in the form

$$\boldsymbol{E}(\boldsymbol{x} - \boldsymbol{x}_c) = \boldsymbol{E}^{\infty} + k\boldsymbol{E}^{(1)}(\boldsymbol{x} - \boldsymbol{x}_c), \tag{7.8}$$

where $\boldsymbol{x}_c$ is the particle centre, and the dimensionless rate-of-strain disturbance field $\boldsymbol{E}^{(1)}$ is available in analytical form from the analysis of Luo & Pozrikidis (2007). Batchelor & Green (1972b) noted that the mean value of $\boldsymbol{E}^{(1)}(\boldsymbol{x} - \boldsymbol{x}_c)$ over a spherical surface centred at $\boldsymbol{x}_c$ is zero; we have confirmed that this is also true when the slip boundary condition applies.

Based on these single-particle results, we expect that, when two equal-sized particles A and B intercept in simple shear flow with the origin set midway such that $\boldsymbol{X}_B = -\boldsymbol{X}_A$, the instantaneous particle stress tensor due to the first particle will be given by

$$\boldsymbol{\Sigma}(\boldsymbol{X}_A) \simeq \alpha_1 \left(\frac{2}{k} \boldsymbol{E}^{\infty} + 2\boldsymbol{E}^{(1)}(2\boldsymbol{X}_A) \right). \tag{7.9}$$

The second term on the right-hand side expresses the effect of the rate-of-deformation field induced by the disturbance flow generated by particle B at the location of particle A. In the chosen frame, the two particles are separated by the distance $2\boldsymbol{X}_A$. Thus, the shearing component of the particle stress tensor is approximately given by

$$\Sigma_{xy}(\boldsymbol{X}_A) \simeq \alpha_1 \left(1 + 2E_{xy}^{(1)}(2\boldsymbol{X}_A) \right). \tag{7.10}$$

Since the velocity due to a force-free particle decays like $1/r^2$ and its derivatives decay like $1/r^3$, when r is distance from the particle centre, the second term on the right-hand sides of the last two equations decays like $1/|\boldsymbol{X}_A|^3$.
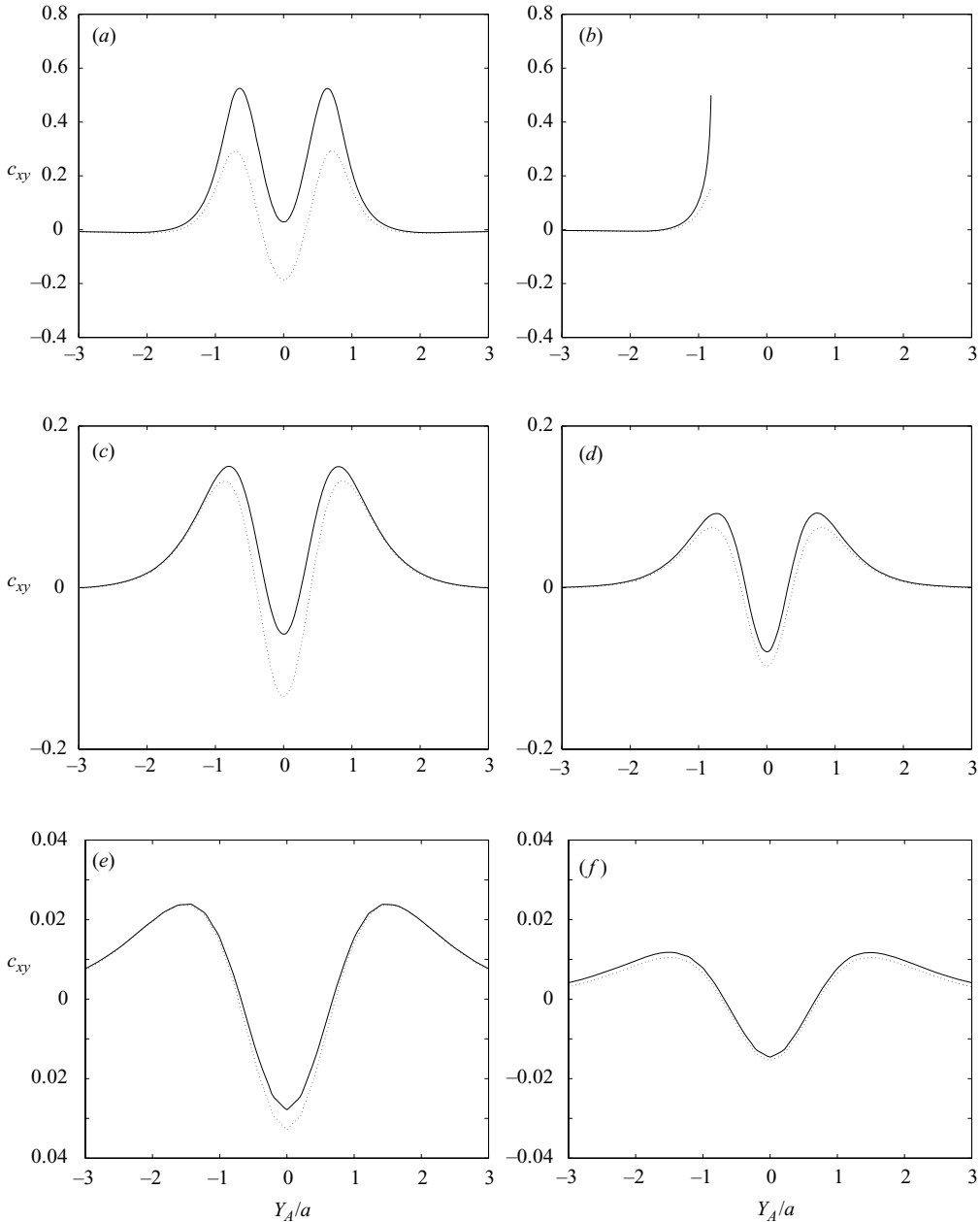
FIGURE 6. Evolution of the scaled particle stress tensor during particle interception in the (X, Y)-plane for initial position $Y_A = -10a$, and (a, b) $X_A = 0.5a$ (c, d) $X_A = a$ (e, f) $X_A = 2a$. The left column is for $\beta = \infty$, and the right column is for $\beta = 0.1$. The dotted lines represent the theoretical prediction $c_{xy} \simeq 2E_{xy}^{(1)}(2X_A)$.

Figure 6 illustrates the evolution of the shifted and normalized shearing component of the particle stress tensor

$$c_{xy}(X_A) \equiv \frac{\Sigma_{xy}(X_A)}{\alpha_1} - 1, \qquad (7.11)$$

for three initial particle positions in the (X, Y)-plane. The dotted lines represent the asymptotic prediction $c_{xy}(X_A) \simeq 2E_{xy}^{(1)}(2X_A)$ deduced from the single-particle analysis. As two spheres with no-slip surfaces approach one another, the particle stress rises to a local maximum, declines, and finally reaches a local minimum when the particles are in the vertical orientation along the X-axis. As the initial position X_{A0} increases from a, to $2a$, c_{xy} decreases nearly by one order of magnitude, confirming the cubic decay. The asymptotic prediction is surprisingly accurate when $X_{A0} = 2a$, but significantly underestimates the particle stress tensor for smaller particle separations. As long as the particles do not collide, allowing for slip does not change the qualitative behaviour, though it significantly reduces the magnitude of the particle stress tensor. When the particles collide, the coefficient c_{xy} tends to a finite value at the collision time, and then follows a different solution branch determined by the unspecified nature of the subsequent motion.

7.3. *Suspension viscosity*

Batchelor & Green (1972b) demonstrated that the particle stress tensor and effective viscosity of a dilute monodisperse suspension can be expanded in an asymptotic series with respect to the particle volume fraction, c,

$$\mu_{\text{eff}} = \mu(1 + \alpha_1 c + \alpha_2 c^2 + \cdots). \tag{7.12}$$

If all particle trajectories originate from infinity, and if the suspension is random and the interceptions are uncorrelated, we are able to compute the coefficient α_2 as a weighted average of the stresslet integrated over time along pairwise interception paths. The basic reasoning is that particle interception makes a contribution to the particle stress tensor that is proportional to the particle volume fraction, c, as well as to the frequency of interception, f.

In the case of simple shear flow, we set the origin such that $X_B = -X_A$ along each interception path, and note that the frequency of interception is given by

$$f(X_{A0}, Z_{A0}) = kn2|X_{A0}|, \tag{7.13}$$

where the subscript 0 denotes the position before interception, and $n = 3c/(4\pi a^3)$ is the particle number density. Next, we compute the cumulative deviation of the stresslet from the single-particle value due to the interception along each path,

$$\bar{\Sigma}_{xy}(X_{A0}, Z_{A0}) \equiv \int_0^\infty (\Sigma_{xy}(t) - \alpha_1) \, \mathrm{d}t. \tag{7.14}$$

Finally, we obtain the contribution of the interception to the shearing component of the particle stress tensor by integrating over all trajectory paths,

$$\Sigma_{xy}^{(2)} = \int_{-\infty}^\infty \int_{-\infty}^\infty f(X_{A0}, Z_{A0}) \bar{\Sigma}_{xy}(X_{A0}, Z_{A0}) \, \mathrm{d}X_{A0} \, \mathrm{d}Z_{A0}. \tag{7.15}$$

Setting

$$\sigma_{xy}^{\text{Eff}} = \mu k \big(1 + c \Sigma_{xy}^{(1)} + c \Sigma_{xy}^{(2)}\big), \tag{7.16}$$

we obtain

$$\alpha_2 = \frac{1}{c} \int_{-\infty}^\infty \int_{-\infty}^\infty f(X_{A0}, Z_{A0}) \bar{\Sigma}_{xy}(X_{A0}, Z_{A0}) \, \mathrm{d}X_{A0} \, \mathrm{d}Z_{A0}$$

$$= \frac{3k}{2\pi a^3} \int_{-\infty}^\infty \int_{-\infty}^\infty |X_{A0}| \bar{\Sigma}_{xy} \, \mathrm{d}X_{A0} \, \mathrm{d}Z_{A0}. \tag{7.17}$$

Batchelor & Green (1972b) computed the coefficient α_2 based on the expression

$$\alpha_2 = \frac{1}{c} \int_{-\infty}^{\infty} \int_{-\infty}^{\infty} \int_{-\infty}^{\infty} (\Sigma_{xy}(\boldsymbol{r}) - \alpha_1) P(\boldsymbol{r}) \, \mathrm{d}r_x \, \mathrm{d}r_y \, \mathrm{d}r_z, \tag{7.18}$$

where $P(\boldsymbol{r})$ is the probability that the centre of sphere A is located at the position $\boldsymbol{X}_B + \boldsymbol{r}$. As $\boldsymbol{r}$ tends to infinity, P reduces to the particle number density, n. Particle conservation requires that P satisfies the Liouville equation

$$\nabla_{\boldsymbol{r}} \cdot (\boldsymbol{V}_A P(\boldsymbol{r})) = 0. \tag{7.19}$$

Integrating this equation over a slender semi-infinite tubular volume bounded on the sides by particle centre trajectories, applying the divergence theorem, and noting that the integrals over the tubular sides vanish identically, we find

$$n2k|X_{A0}| \, \mathrm{d}X_{A0} \, \mathrm{d}Y_{A0} = P(\boldsymbol{r}) \boldsymbol{V}_A \cdot \boldsymbol{t} \, \mathrm{d}S, \tag{7.20}$$

where $\mathrm{d}S$ is the area of the tube cross-section on the downstream end located at $\boldsymbol{r}$, and $\boldsymbol{t}$ is the unit tangential vector along the tube centreline. Thus,

$$\alpha_2 = \frac{2kn}{c} \int_{-\infty}^{\infty} \int_{-\infty}^{\infty} \int_{-\infty}^{\infty} |X_{A0}|(\Sigma_{xy}(\boldsymbol{r}) - \alpha_1) \frac{1}{\boldsymbol{V}_A \cdot \boldsymbol{t}} \frac{\mathrm{d}r_x \, \mathrm{d}r_y \, \mathrm{d}r_z}{\mathrm{d}S} \, \mathrm{d}X_{A0} \, \mathrm{d}Y_{A0}. \tag{7.21}$$

The fraction of the four differentials on the right-hand side is the differential arclength along $\boldsymbol{t}$, denoted by $\mathrm{d}l$. Now we identify the ratio $\mathrm{d}l/\boldsymbol{V}_A \cdot \boldsymbol{t}$ with the time interval $\mathrm{d}t$, and recover precisely (7.17).

We return to (7.17) and recall that, when the trajectories are well-separated, $\Sigma_{xy}(t) - \alpha_1 \simeq 2\alpha_1 E_{xy}^{(1)}$, and

$$\bar{\Sigma}_{xy} \sim a^3 \int_{-\infty}^{\infty} \frac{\mathrm{d}t}{\left(X_A^2 + Y_A^2 + Z_A^2\right)^{3/2}}. \tag{7.22}$$

Because the particles are nearly convected with the velocity of the simple shear flow, $\mathrm{d}Y_A/\mathrm{d}t \simeq kX_A$,

$$\bar{\Sigma}_{xy} \sim \frac{a^3}{k|X_{A0}|} \int_{-\infty}^{\infty} \frac{\mathrm{d}Y_A}{\left(X_{A0}^2 + Y_A^2 + Z_{A0}^2\right)^{3/2}} \sim \frac{a^3}{k|X_{A0}|\left(X_{A0}^2 + Z_{A0}^2\right)}. \tag{7.23}$$

Substituting in (7.17) we obtain a non-convergent integral in the $X_{A0} - Y_{A0}$ plane. Batchelor & Green (1972b) encountered a similar difficulty working in the framework of configurational probability, which they overcame by renormalization.

We follow essentially the same approach by recalling that the mean value of $\boldsymbol{E}^{(1)}(\boldsymbol{x} - \boldsymbol{x}_c)$ over the surface of a sphere centred at $\boldsymbol{x}_c$ is zero and writing the identity

$$\int_{-\infty}^{\infty} \int_{-\infty}^{\infty} \bar{\boldsymbol{E}}^{(1)}(2X_{A0}, 2Z_{A0}) \, \mathrm{d}X_{A0} \, \mathrm{d}Z_{A0} = \boldsymbol{0}, \tag{7.24}$$

where

$$\bar{\boldsymbol{E}}^{(1)}(2X_{A0}, 2Z_{A0}) \equiv \int_{-\infty}^{\infty} \boldsymbol{E}^{(1)}(2X_{A0}, 2Y_A, 2Z_{A0}) \, \mathrm{d}Y_A. \tag{7.25}$$

We may now state without any approximation

$$\alpha_2 = \frac{3}{2\pi a^2} \int_{-\infty}^{\infty} \int_{-\infty}^{\infty} \Phi(X_{A0}, Z_{A0}) \, \mathrm{d}X_{A0} \, \mathrm{d}Z_{A0}, \tag{7.26}$$
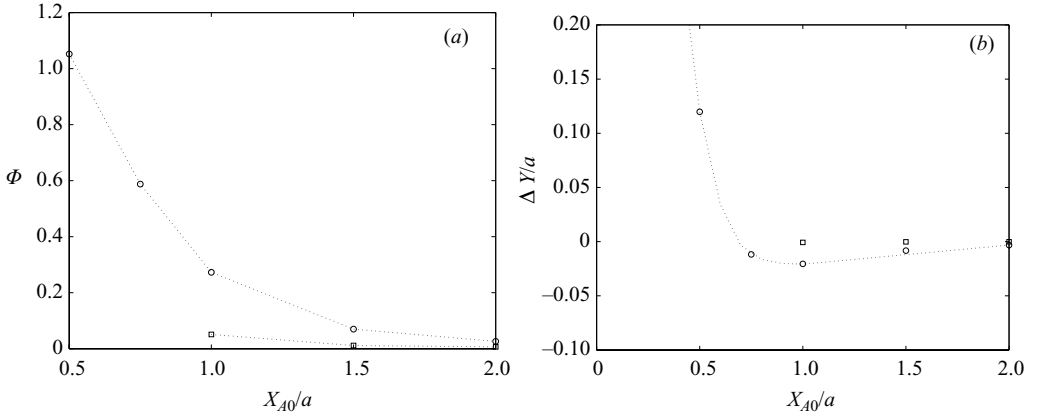
FIGURE 7. Effect of the slip coefficient on (*a*) the dimensionless function Φ, and (*b*) net longitudinal shift for particle trajectories in the (X, Y)-plane. The circles correspond to $\beta = \infty$ (no-slip), and the squares correspond to $\beta = 0.1$.

where

$$\Phi(X_{A0}, Z_{A0}) \equiv \frac{\alpha_1}{a} \left[\frac{k|X_{A0}|}{\alpha_1} \bar{\Sigma}_{xy}(X_{A0}, Z_{A0}) - 2\,\bar{E}^{(1)}_{xy}(2X_{A0}, 2Z_{A0}) \right] \qquad (7.27)$$

is a dimensionless integrand. When the trajectories are well-separated, $\mathrm{d}Y_A/\mathrm{d}t \simeq k|X_{A0}|$, and

$$\Phi(X_{A0}, Z_{A0}) \simeq \frac{\alpha_1}{a} \int_{-\infty}^{\infty} \left[\frac{1}{\alpha_1} \Sigma_{xy}(X_{A0}, Y_A, Z_{A0}) - 1 - 2E^{(1)}_{xy}(2X_{A0}, 2Y_A, 2Z_{A0}) \right] \mathrm{d}Y_A. \quad (7.28)$$

Because of (7.10), the function $\Phi(X_{A0}, Z_{A0})$ decays faster than $1/(X_{A0}^2 + Z_{A0}^2)$, leading to a convergent integral.

The function Φ may be computed by integrating the particle stress tensor along particle trajectories and the function $E^{(1)}_{xy}(2X_{A0}, 2Y_A, 2Z_{A0})$ along paths parallel to the Y axis. In our calculations, the particle motion in the (X, Y) plane was integrated from $Y_A = -10a$ to $10a$. At the end of a simulation, the X position of a particle centre differs only by an amount on the order of $10^{-5}a$ from the initial position due to the numerical error. Figure 7(*a*) shows a graph of Φ plotted against X_{A0} for $\beta = \infty$ (no-slip) and 0.1. The data clearly suggests that allowing for slip considerably reduces the magnitude of Φ and thus the value of the second-order viscosity coefficient α_2. It is striking that, as the slip coefficient decreases from infinity to zero, the magnitude of Φ drops by one order of magnitude.

The contribution to the stresslet from the closed trajectory paths lying inside the shaded area in figure 5(*b*) must also be considered. Batchelor & Green (1972*b*) explain that the problem is indeterminate, as the percentage of particle pairs permanently engaged in cyclic motion cannot be assessed without further assumptions. However, there are circumstances where closed trajectories are eliminated after a certain evolution time due to particle surface roughness, as discussed in Wilson & Davis (2000). These physical conditions are favourable in that particle roughness also introduces an effective slip velocity included in our formulation. Thus, the conclusions reached on the basis of the open-trajectory analysis are most likely to prevail in a real flow environment.

7.4. *Longitudinal particle self-diffusivity*

After a non-colliding interception, a particle resumes its initial position in the (X, Y) plane, exhibiting no net migration. However, the particle does experience an overall drift in the longitudinal position Y compared to that corresponding to the unperturbed straight path, defined as

$$\Delta Y \equiv Y_A(t \to \infty) - Y_A(t = 0) - kX_{A0}t. \tag{7.29}$$

When the particle number density distribution is uniform in a region that is large compared to the particle size, a particle will experience a large number of interceptions while remaining in an essentially unchanged environment. By symmetry, the mean value of ΔY is zero, as a particle intercepting with another particle from above or below is, respectively, delayed or pushed forward. If the interceptions are uncorrelated, we may use the theory of random walks to describe the statistics of the streamwise particle position in terms of a long-time longitudinal self-diffusivity defined as

$$D_{YY} = \int_{-\infty}^{\infty} \int_{-\infty}^{\infty} f(X_{A0}, Y_{A0}) \Delta Y^2 \, dX_{A0} \, dY_{A0}, \tag{7.30}$$

with the understanding that $X_B = -X_A$. Consideration of the far-field behaviour shows that this integral is convergent.

Figure 7(*b*) shows a graph of ΔY plotted against X_{A0} for $\beta = \infty$ (no-slip) and 0.1. The dotted lines were constructed using the analytical solution for no-slip surfaces discussed in the Appendix. Our numerical results for no-slip surfaces represented by the circles are in excellent agreement with these predictions. For small particle separations ΔY is positive, whereas for large particle separations ΔY is negative. The data suggests that allowing for surface slip reduces the magnitude of ΔY and thus the value of the longitudinal self-diffusivity.

8. Discussion

We have developed a numerical method for computing with high accuracy linear flow past a pair of spherical particles with no-slip or slip surfaces. The key step is the Fourier expansion of the flow variables with respect to the meridional angle measured around the axis connecting the particle centres at every instant. We have found that only the zeroth and first Fourier coefficients are necessary for computing the force, torque, translational and angular velocities. The second Fourier coefficients are necessary for evaluating the stresslet and thus investigating the structure of the far flow and the rheology of a dilute suspension.

Simulations were performed for particles of equal size intercepting in simple shear flow. It was found that, when the slip coefficient is sufficiently small, the inter-particle gap may become zero and the particles may come in physical contact at a finite time. Collision occurs when the particles intercept in a plane that is normal to the vorticity of the simple shear flow (XY-plane), as well as for more general configurations. The critical value of the slip coefficient depends on the relative initial particle positions. When the particles intercept in the XY-plane, the threshold initial height along the X axis above which collision does not occur under any circumstances is bracketed by $0.8\,a$ and a, where a is the particle radius.

To pursue the motion after collision, it is necessary to specify the nature of the particle contact. Some particles may firmly adhere and move as rigid doublets until separated by a pulling hydrodynamic force. Other particles may roll over one another while in contact. Davis *et al.* (2003) studied the translational and rotational motion of

a suspended sphere with microscopic roughness falling past a lighter sphere or moving down an inclined surface, and observed roll-slip behaviour. With straightforward modifications, the boundary-integral method implemented in our work should be able to describe these motions.

Our analysis is complementary to that of Wilson & Davis (2000, 2002) and Davis *et al.* (2003) on the motion of particles with rough surfaces, in that our formulation accounts for the slip velocity, possibly associated with surface roughness, whereas their formulation accounts for the effect of surface irregularities during collision. If we assume that the slip length is comparable to the length scale of the surface roughness, $\mathscr{L}$, we find $\beta = L/\mathscr{L}$. In laboratory experiments, natural or fabricated surface roughness corresponds to values of β in the range 100–1000. Our results indicate that this level of roughness will have a significant effect on intercepting particle trajectories.

We have monitored the behaviour of the particle stress tensor during the interception, and found that an asymptotic prediction based on the one-particle solution is surprisingly accurate for particle positions along the X-axis as small as two particle radii, but significantly underestimates the particle stress tensor for smaller particle separations. The results showed that, as long as the particles do not collide, allowing for slip does not change the qualitative behaviour, and only reduces the magnitude of the particle stress tensor. When the particles collide, the stresslet tends to a finite value at the collision time, and then follows a different solution branch determined by the unspecified nature of the subsequent motion.

We have considered the effective viscosity of a dilute suspension and discussed two equivalent methods of calculating the coefficient of the quadratic term in the asymptotic expansion with respect to the particle volume fraction. Our computations suggest that allowing for slip considerably reduces the value of this coefficient. In particular, as the slip coefficient decreases from infinity to zero, the magnitude of this coefficient drops by one order of magnitude. These results have significant implications on the effective rheology of suspensions of rough and irregular particles.

Random interceptions modify the longitudinal particle positions after an event, and the net effect can be described in terms of a longitudinal self-diffusivity. Our results showed that particle slip reduces the magnitude of the longitudinal self-diffusivity by allowing the particles to roll over one another more easily during the interception. Because interceptions do not modify the transverse particle positions after an event, computation of the transverse self-diffusivity requires consideration of particle triplet interceptions, which is beyond the capability of our methods.

The numerical method for the two-particle problem proposed in this work can be incorporated in a more general framework, wherein pairwise interactions in a non-dilute suspension are subtracted off and treated in particle doublet coordinates, whereas multi-particle interactions are treated by domain discretization methods or multi-pole expansions. In essence, this amounts to accounting for strong lubrication forces based on the pairwise interaction model. The strength of this approach is that results with a specified level accuracy can be obtained, albeit at a yet undetermined computational cost.

Appendix. Interception of two no-slip spheres

Expressions for the trajectories of two identical particles of radius a intercepting in simple shear flow with shear rate k are summarized by Kim & Karrila (1991). The

differential equations governing the evolution of the distance between the particle centres are

$$\dot{x} = k\left(y + ex - \tfrac{1}{2}By\right), \quad \dot{y} = k\left(ey - \tfrac{1}{2}Bx\right), \quad \dot{z} = kez, \qquad \text{(A 1)}$$

where $\boldsymbol{x} = (\boldsymbol{X}_c^{(2)} - \boldsymbol{X}_c^{(1)})/a$, $e = xy(B - A)/r^2$, and $r = |\boldsymbol{x}|$. The mobility functions A and B are given by

$$\left.\begin{aligned}
A &= 5r^{-3} - 8r^{-5} + 25r^{-6} - 35r^{-8} + 125r^{-9} - 102r^{-10} + 12.5r^{-11} + 430r^{-12}, \\
B &= \tfrac{1}{3}(16r^{-5} + 10r^{-8} - 36r^{-10} - 25r^{-11} - 36r^{-12}),
\end{aligned}\right\} \tag{A 2}$$

in the far field $r \geqslant 2.5$,

$$\left.\begin{aligned}
A &= -4.3833 + 17.7176r^{-1} + 14.8204r^{-2} - 92.4471r^{-3} - 46.3151r^{-4} + 232.2304r^{-5}, \\
B &= -3.1918 + 12.3641r^{-1} + 11.4615r^{-2} - 65.2926r^{-3} - 36.4909r^{-4} + 154.8074r^{-5},
\end{aligned}\right\} \tag{A 3}$$

in the intermediate regime, $2.01 < r < 2.5$, and

$$A = \frac{16.3096}{r} - 7.1548, \qquad B = 2\,\frac{0.4056\,C^2 + 1.49681\,C - 1.9108}{r(C^2 + 6.04250\,C + 6.32549)}, \qquad \text{(A 4)}$$

in the lubrication regime, $2 < r \leqslant 2.01$, where $C = -\ln(r - 2)$.

REFERENCES

BASSET, A. B. 1888 *A Treatise on Hydrodynamics*. Cambridge University Press (Reprinted by Dover, 1961).

BATCHELOR, G. K. 1970 The stress system in a suspension of force-free particles. *J. Fluid Mech.* **41**, 545–570.

BATCHELOR, G. K. & GREEN, J. T. 1972a The hydrodynamic interaction of two small freely-moving spheres in a linear flow field. *J. Fluid Mech.* **56**, 375–400.

BATCHELOR, G. K. & GREEN, J. T. 1972b The determination of the bulk stress in a suspension of spherical particles to order c^2. *J. Fluid Mech.* **56**, 401–427.

BEAVERS, G. S. & JOSEPH, D. D. 1967 Boundary conditions at a naturally permeable wall. *J. Fluid Mech.* **30**, 197–207.

BLACK, W. B. & GRAHAM, M. D. 2001 Slip, concentration fluctuations and flow instability in sheared polymer solutions. *Macromolecules* **34**, 5731–5733.

CERCIGNANI, C. 2000 *Rarefied Gas Dynamics*. Cambridge University Press.

CICHOCKI, B., FELDERHOF, B. U. & SCHMITZ, R. 1988 Hydrodynamic interactions between two spherical particles. *Physicochem. Hydrodyn.* **10**, 383–403.

DAVIS, R. H., ZHAO, Y., GALVIN, K. P., & WILSON, H. J. 2003 Solid–solid contacts due to surface roughness and their effects on suspension behaviour. *Phil. Trans. R. Soc. Lond.* A **361**, 871–894.

EINSTEIN, A. 1906 Eine neue Bestimmung der Moleküledimensionen. *Annalen Phys.* **19**, 289–306.

FELDERHOF, B. U. 1976a Force density on a sphere in linear hydrodynamics. I. Fixed sphere, stick boundary conditions. *Physica* A **84**, 557–568.

FELDERHOF, B. U. 1976b Force density on a sphere in linear hydrodynamics. II. Moving sphere, mixed boundary conditions. *Physica* A **84**, 569–576.

FELDERHOF, B. U. & JONES, R. B. 1986 Hydrodynamics scattering theory of flow about a sphere. *Physica* A **136**, 77–98.

HOCKING, L. M. 1973 The effect of slip on the motion of a sphere close to a wall and of two adjacent spheres. *J. Engng. Math.* **7**, 207–221.

JONES, R. B. & SCHMITZ, R. 1988 Mobility matrix for arbitrary spherical particles in solution. *Physica* A **149**, 373–394.

KIM, S. & KARRILA, S. J. 1991 *Microhydrodynamics: Principles and Selected Applications.* Butterworth–Heinemann.

LUO, H. & POZRIKIDIS, C. 2007 Effect of slip on the motion of a spherical particle in infinite flow and near a plane wall. *J. Engng Maths* (Submitted).

MAXWELL, J. C. 1879 On stresses in rarefied gases arising from inequalities of temperature. *Phil. Trans. Roy. Soc. Lond.* **170**, 231–256.

NAVIER, C. L. M. H. 1823 Mémoire sur les lois du mouvement des fluides. *Mémoires de l'Académie Royale des Sciences de l'Institut de France* **VI**, 389–440.

POZRIKIDIS, C. 1992 *Boundary Integral and Singularity Methods for Linearized Viscous Flow.* Cambridge University Press.

SCHAAF, S. A. & CHAMBRE, P. L. 1961 *Flow of Rarefied Gases.* Princeton University Press.

SCHMITZ, R. & FELDERHOF, B. U. 1978 Creeping flow about a sphere. *Physica* A **92**, 423–437.

SCHMITZ, R. & FELDERHOF, B. U. 1982a Creeping flow about a spherical particle. *Physica* A **113**, 90–102.

SCHMITZ, R. & FELDERHOF, B. U. 1982b Friction matrix for two spherical particles with hydrodynamic interaction. *Physica* A **113**, 103–116.

SCHMITZ, R. & FELDERHOF, B. U. 1982c Mobility matrix for two spherical particles with hydrodynamic interaction. *Physica* A **116**, 163–177.

TAYLOR, G. I. 1932 The viscosity of a fluid containing small drops of another liquid. *Proc. R. Soc. Lond.* A **138**, 41–48.

VINOGRADOVA, O. I. 1999 Slippage of water over hydrophobic surfaces. *J. Miner. Proc.* **56**, 31–60.

WILSON, H. J. & DAVIS, R. H. 2000 The viscosity of a dilute suspension of rough spheres. *J. Fluid Mech.* **421**, 339–367.

WILSON, H. J. & DAVIS, R. H. 2002 Shear stress of a monolayer of rough spheres. *J. Fluid Mech.* **452**, 425–441.